Title
A comparative study on the auto-ignition of non-premixed dimethyl ether and ethanol counterflow flames

Permalink
https://escholarship.org/uc/item/7nj3h45k

Author
Aksoy, Sukru Taha

Publication Date
2022

Peer reviewed|Thesis/dissertation

UNIVERSITY OF CALIFORNIA SAN DIEGO

A comparative study on the auto-ignition of non-premixed dimethyl ether and ethanol counterflow flames

A thesis submitted in partial satisfaction of the
requirements for the degree Master of Science

in

Mechanical and Aerospace Engineering

by

Sukru Taha Aksoy

Committee in charge:

Professor Kalyanasundaram Seshadri, Chair
Professor Forman A. Williams, Co-Chair
Professor Saha Abhishek

2022

The thesis of Sukru Taha Aksoy is approved, and it is acceptable in quality and form for publication on microfilm and electronically.

University of California San Diego

2022

TABLE OF CONTENTS

LIST OF FIGURES

LIST OF TABLES

ACKNOWLEDGEMENTS

I would like to thank all the people who directly or indirectly supported me during my MSc thesis. First, I want to sincerely thank my advisor, Prof. Kalyanasundaram Seshadri for his guidance, trust, and encouragement. His experience and knowledge has kept me in the right direction. I am extremely grateful for his supervision in work and understanding in off-work difficulties, that have made this MSc possible. I would also like to thank my dissertation committee members, Prof. F. A. Williams and Prof. S. Abishek for their valuable feedback and discussions related to my MSc work.

I would like to thank all my colleagues for their active collaboration, continuous support, and the good memories. It was a privilege to work with and along-side them. I am grateful to all of them, but I would also like to give special thanks to Liang Ji, without whom my research would have no doubt taken fives times as long. It is his support that helped me in an immeasurable way.

Most importantly, I owe so much to my parents and all my family for their unconditional, unending love, understanding, and patience that helped me navigate through the difficult moments during the last years. Finally, I thank all my friends whose constant support and liveliness kept me going everyday.

ABSTRACT OF THE THESIS

A comparative study on the auto-ignition of non-premixed dimethyl ether and ethanol counterflow flames

by

Sukru Taha Aksoy

Master of Science in Mechanical and Aerospace Engineering

University of California San Diego 2022

Professor Kalyanasundaram Seshadri, Chair
Professor Forman A. Williams, Co-Chair

In this study, combustion behaviors and characteristics of ethanol, dimethyl ether (DME) and their blends are investigated. Dimethyl ether and ethanol, the two fuels used for the study, are isomers of C_2H_6O, which have the same molecular formula but distinct chemical structures. The goal is to investigate and comprehend the differences, similarities and their interaction in fuel mixtures. The chemical kinetic software tool Cantera is used for numerical computations in the study. Prior experimental research data are reproduced and detailed analyses are conducted. Counterflow diffusion flame simulations are employed in the study as the experimental research utilizes a counterflow burner design. Auto-ignition simulation studies are conducted using San

Diego mechanism as chemical kinetic mechanism. The San Diego Mechanism is a condensed chemical-kinetic mechanism utilized in combustion modeling applications, and it is developed and hosted by the University of California San Diego combustion group. For the computational studies a sub-mechanism for dimethyl ether(DME) is implemented to the main mechanism. Across the simulations, fuels with various partial percentages are used but the overall mass fraction remained constant at 0.4. For each fuel mixture, the oxidizer stream's temperature at autoignition is noted. Additionally, thorough investigations of the heat release rate analyses and reaction rate analyses are done to identify the dominant reactions in various mixtures. Low and high strain rate analyses are elucidated considering the dominant reactions identified in the heat release rate analyses and reaction rate analyses. In low strain rate analyses, there is a series of reactions related from CH_3OCH_3(DME) with OH. The decrease of DME in the mixtures and increasing competition of OH from ethanol decreases the magnitude of heat release. High strain rate analyses show that, the dominance of ethanol related reaction, CH_3CHOH reacts with O_2, decreases from pure ethanol to pure DME. On the other hand, the additional DME reacts with OH which increases its dominance.

Chapter 1

Introduction

1.1 Overview

The non-premixed flame of ethanol and dimethyl ether(DME) is the focus of this research. For the two alternative fuels and various mixes of them, the critical conditions of autoignition are investigated using experimental data and data from computational simulations. The research group supervised by Prof. Kalyanasundaram Seshadri at the University of California, San Diego, acquired the experimental results of autoignition and extinction of the various fuel compositions of Dimethyl-ether(DME)/Ethanol blends[1]. The thesis begins with an introduction to counterflow diffusion flames. Experiments and the experimental setup is explained in detail. Reaction mechanisms including the sub-mechanisms of the alternative fuels used in the experiments, are mentioned. In particular, the San Diego mechanism, developed by the combustion group directed by Prof. Forman A. Williams, Prof. Kalyanasundaram Seshadri and Prof. Robert Cattolica [2]. The software program Cantera, is used to conduct numerical simulations to comprehend the combustion behaviours of the fuels[3]. Numerical studies for defining the critical conditions of autoignition, heat release analyses and investigations into reaction rates are all carried out. Heat release bar graphs and reaction rate plots are used to demonstrate and evaluate the dominant reactions for different fuel mixtures, including pure ethanol and pure dimethyl ether. The thesis concludes with discussions of the results, along with ideas for possible future study topics. The reactions of the San Diego mechanism can be found in Appendix A.

1.2 Scope of Study

The goal of the study is to elucidate the combustion behavior of dimethyl ether(DME) and ethanol mixtures under low and high strain rate conditions. It is aimed to simulate the critical conditions for autoignition. During the simulations San Diego mechanism is used, which is developed by a group at University of California, San Diego. It is established through a comparison of the simulation results with the existing experimental data that the San Diego mechanism simulation results for autoignition that they are compatible with the experiment. These studies contribute to a thorough understanding of the interactions between ethanol and dimethyl ether and their mixtures, which could be useful for the usage of these isomers as alternative fuels.

1.3 Outline of Thesis

This study is a comparative study on the autoignition of non-premixed dimethyl ether and ethanol counterflow diffusion flames. The thesis starts with an introduction about diffusion flames and counterflow diffusion flame configuration. Also a brief explanation of chemical reaction mechanisms and the experiment that is used to compare with simulation data. Following the experiment introduction the experimental setup is also explained in detail. Cantera, which is the software tool used in numerical simulations is represented. Formulation of the simulations, calculations and procedure is discussed. Finally the results for simulations are discussed. Starting with the autoignition results, considering that it is examined as low strain rate autoignition analysis and high strain rate autoignition analysis separately. Last part is about the conclusion and future work.

Chapter 2

Counterflow Diffusion Flames

Counterflow flames are divided in two configurations, premixed flames and non-premixed flames. Counterflow non-premixed or also called diffusion flames are the ones that occur when the flow of fuel and air is parallel and in the opposite directions. Laminar counterflow diffusion flames offer a plethora of significant knowledge regarding the fundamental characteristics of non-premixed combustion. In terms of research studies and experimental use, non-premixed flames are more practical than premixed flames.

About the formation of the counterflow diffusion flames, when the two opposing streams collide, a perpendicular plane arises where the momentum of the fuel side and the momentum of the air side interact and generate a stagnation plane. The momentum ratio between the fuel stream and the oxidizer stream determines the position of the stagnation plane.

Stochiometric plane refers to the plane where a flame is forming as a result of the reactions between the fuel and oxidizer. This is the position where the diffusion fluxes of oxidizer and fuel are balanced.

The flame appears to be a flat disc since the streams are flowing from cylindrical nozzles, creating an axisymmetric flows. As a result of the flow properties, the flame is considered as relatively one-dimensional. Detailed explanation about the one dimensionality and equations can be found at Section 2.3. Due to the fact that they exhibit a diffusion flame structure that is one dimensional, counterflow diffusion flames are frequently used in experiments. Counterflow burners are the equipment to create counterflow flames. The duration of the chemical reaction and the velocity of the fuel and oxidizer flows are the key determinants of combustion in counter flow burners [4].

The counter flow configuration is shown schematically in figure 2.1. In the illustration 2.1, two opposing streams can be seen. The stream exiting the fuel duct is referred as the fuel stream, and the stream exiting the oxidizer duct is defined as the oxidizer stream. The flow assumptions that make the counterflow configuration calculations practical, are that the flow is steady, laminar and axisymmteric.

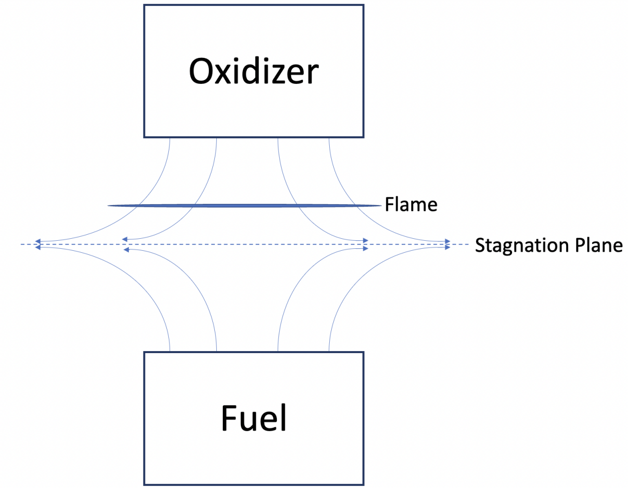

Figure 2.1. Counter flow configuration illustrated schematically.

2.1 Strain Rate

The normal gradient of the normal component of flow velocity is defined as the strain rate. The strain rate is computed utilizing each stream's velocity for oxidizer and fuel streams. In this study one will focus on oxidizer strain rate. The equation for calculating the oxidizer strain rate is given at equation (2.1)

$$a_2 = \frac{2|V_2|}{L}\left(1+\frac{|V_1|\sqrt{\rho_1}}{|V_2|\sqrt{\rho_2}}\right) \tag{2.1}$$

At equation (2.1) the subscript "$_1$" corresponds to the fuel side and subscript "$_2$" refers to the oxidizer side. V_1 $[\frac{m}{s}]$ and V_2 $[\frac{m}{s}]$ are respectively the normal components of the stream velocities for fuel duct and oxidizer duct. L $[m]$ denotes for the distance between the ducts of the counterflow burner. The oxidizer strain rate a_2 can be calculated using the equation (2.1). This oxidizer strain rate equation is derived using asymptotic theory in with the assumption that the laminar flows at the duct outlets have high Reynolds number values. [5]

$$\rho_1 V_1^2 = \rho_2 V_2^2 \tag{2.2}$$

Equation (2.1) can be simplified and reduced to (2.3) using the momentum balance equation (2.2). Thanks to the reduced equation (2.3), the oxidizer strain rate can be calculated using the velocity of oxidizer flow and the distance between ducts.

$$a_2 = \frac{4V_2}{L} \tag{2.3}$$

2.2 Damköhler Number

Damköhler number, Da introduced by Gustave Damköhler, is defined as the fraction of the flow time to reaction time. Flow time is regarded as characteristic aerodynamic time, t_a. Reaction time is the characteristic chemical time, t_c which includes the convection and diffusion process. Chemical time, t_c is reliant on the fuel and determines the reactivity of the fuel. Reactant transport and mixing time, t_a is influenced by the flow field's characteristics.

$$Da = \frac{t_a}{t_c} \tag{2.4}$$

If one consider two edges of the Damköhler number, low Damköhler number, $Da \ll 1$, signifies slow chemical reactions and high Damköhler number, $Da \gg 1$, signifies rapid chemical reactions. When diffusion flames are taken into account, the Damköhler number is high due to the nominator of the Damköhler number, t_a, mixing and transport duration is very large.

Strain rate could be used to control the Damköhler number. For instance, increasing the strain rate results in a rise in velocity, as can be remembered from the equation (2.3). Increased velocity means that the flow time will decrease which is one of the two parameters of the Damköhler number. In other words, one could conclude that the Damköhler number can be controlled by altering the strain rate.

2.3 Governing Equations of Counterflow Diffusion Flames

This section covers the governing equations used to compute one dimensional counterflow diffusion flames.

The one dimensional flame solution procedure is also used in the source codes of Cantera. Simulations conducted in this thesis are based on these calculations and procedure. The axisymmetric flow geometry is depicted in figure 2.2. Across the variables of the governing equations; u corresponds to the axial velocity, v corresponds to the radial velocity, T as temperature and Y_k is the mass fraction of species k. Boundaries are located at $z = 0$ and $z = L$. The variables u, T and Y_k are independent of r which means their partial derivatives of radial direction in the governing equations can be eliminated. The radial velocity is linear in direction r and usually zero. The mach number is very low, so pressure variable P is nearly constant. Considering the limits one can say: $Ma \ll 1$ and $\frac{L}{D} \ll 1$. Λ in the pressure equation of equation (2.5) is a constant, identified as a component of the solution.

$$u = u(z), \quad v = rV(z), \quad T = T(z), \quad Y_k = Y_k(z), \quad P = P_0 + \Lambda \frac{r^2}{2} \tag{2.5}$$

Governing flow equations reduce from partial derivative equations(PDE) to ordinary derivative equations(ODE) when similarity solution is applicable[6],[7]. After the elimination process using the assumptions coming from the conditions. The governing equations reduce to only in axial coordinate z where the continuity equation can be seen in equation (2.6), momentum equation in equation (2.7), species equation in equation (2.8) and energy equation in equation (2.9) [8].

$$Continuity: \quad \frac{\mathrm{d}}{\mathrm{d}z}(\rho u) + 2\rho V = 0 \tag{2.6}$$

$$Radial\ Momentum: \quad \rho\frac{\mathrm{d}V}{\mathrm{d}t} = \frac{\mathrm{d}}{\mathrm{d}z}\left(\mu\frac{\mathrm{d}V}{\mathrm{d}z}\right) - \Lambda - \rho u\frac{\mathrm{d}V}{\mathrm{d}z} - \rho V^2 \tag{2.7}$$

$$Species: \rho\frac{\mathrm{d}Y_k}{\mathrm{d}t} = -\rho u\frac{\mathrm{d}Y_k}{\mathrm{d}z} - \frac{\mathrm{d}j_k}{\mathrm{d}y} + W_k\dot{w}_k \tag{2.8}$$

$$Energy: \rho c_p\frac{\mathrm{d}T}{\mathrm{d}t} = -\rho c_p u\frac{\mathrm{d}T}{\mathrm{d}z} + \frac{\mathrm{d}}{\mathrm{d}z}\left(\lambda\frac{\mathrm{d}T}{\mathrm{d}z}\right) - \sum W_k\dot{w}_k h_k - \sum j_k c_{p,k}\frac{\mathrm{d}T}{\mathrm{d}z} \tag{2.9}$$

Finite Difference Methods (FDM) are methods used to solve differential equations numerically. For various terms, Cantera employs the following numerical finite difference techniques. Upwind finite difference method is used for convective terms; $\frac{\mathrm{d}V}{\mathrm{d}z}$, $\frac{\mathrm{d}Y_k}{\mathrm{d}z}$ and $\frac{\mathrm{d}T}{\mathrm{d}z}$. For the diffusive terms in the governing equation 1 central difference method is used as numerical method.

The fuel and oxidizer properties needs to be provided and after defining the solution domain and boundary conditions, these differential equations (2.6), (2.7), (2.8) and (2.9) are solved numerically as described above, to compute one dimensional flame solutions.

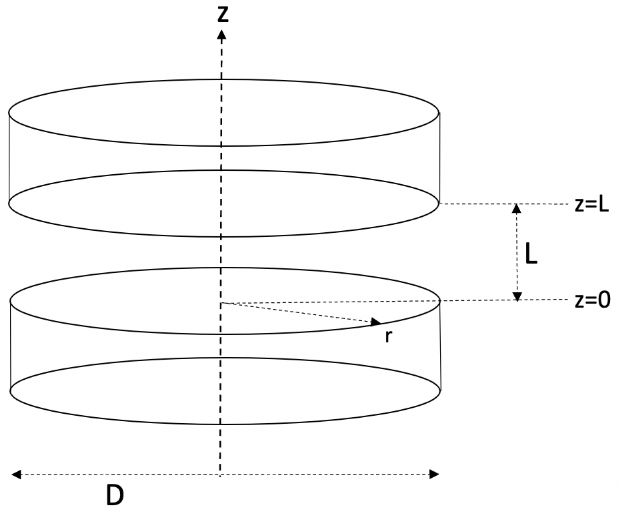

Figure 2.2. Axisymmetric flow geometry of Counterflow Configuration

Chapter 3

Reaction Mechanisms

A reaction mechanism—also known as a chemical-kinetic mechanism—is a set of elementary reactions between distinct species that are shown to take place during combustion of a fuel. In complex series of reactions, step wise sequences of reactions occur. Every single reaction, referred to as an elementary reaction, consists of one, two molecules, or radicals. The reactions mechanism is the general pattern of elementary reactions. The rate of a reaction typically changes when the concentration of the components involved changes and also with temperature and pressure changes. Mathematically, this effect is demonstrated via a rate equation. All reactions have a step or elementary reaction that determines their rate which is can be also called elementary rate-determining process. All the species engaged in elementary processes including this step are included in the rate equation. As a reaction develops, the concentrations of the reactants and products change, which causes the reaction's rate to change as well. This also implies that the rate of a reaction can be determined in terms of the reduction of the reactant concentrations or the enrichment of the product concentrations. Rate Laws or Rate Equations are terms used to describe the formulations and relationships. The key to developing a mechanism is the rate at which the reactants are turned into products as well as figuring out the various ways that each species is produced and consumed.

There are different mechanisms which are including the species DME & Ethanol. Alternatively, it is possible to implement sub-mechanisms to previously developed reaction mechanisms to involve different species. Naming a few of them; a thorough chemical kinetic mechanism was created and verified by comparison to experiment results by Lawrence Livermore National Laboratory(LLNL), the mechanism of National University of Ireland, Galway named AramcoMech and lastly the San Diego Mechanism built on the principle of reducing the number of species, developed by the University of California, San Diego.

3.1 DME & Ethanol Mechanisms

Several mechanisms have been developed for the species DME and ethanol by diverse groups all over the world. The San Diego Mechanism, which was developed to be a relatively short mechanism for use in situations where larger mechanisms become impracticable due to the fact that larger mechanisms need hundreds of rate constants. Numerical simulations using the San Diego Mechanism are done in this study, to see the analogy between the experiment results and the San Diego Mechanism numerical computations.

3.1.1 San Diego Mechanism

San Diego Mechanism was developed with the aim of lowering the number of species and, consequently, the quantity of reactions for combustion researches. It is a viable choice among chemical kinetic mechanisms, particularly when operating larger mechanisms would take too much time. The San Diego mechanism is used to perform kinetic modeling of the two fuels, ethanol and dimethyl ether in this study. Reactions relevant to ethanol combustion are first introduced to the existing San Diego Mechanism in 2004 [9]. Later, further revisions and enhancements to the ethanol chemistry and combustion are done. Saxena et al. [10] has more information on the oxidation and decomposition of ethanol. Dimethyl ether, was also not included in the San Diego mechanism. In the work of J.C. Prince and F.A. Williams [11] , the fundamental San Diego Mechanism remained unaltered. The combustion of DME and its mixes with C1-C3 alkanes is successfully simulated with just the essential reaction additions. The mechanism includes the essential species and reactions for the simulations after the implementation of a sub-mechanism for DME. San Diego sub-mechanism for DME is a short kinetic mechanism involving 5 species and 14 reactions[12]. The elementary steps for DME sub-mechanism can be seen in table 3.1. Detailed information about the decomposition of dimethyl ether can be found in the research of J.C. Prince and F.A. Williams [11]. Despite being a relatively brief sub-mechanism, it is remarkably beneficial due its due to its usefulness and simple structure. Accordingly complete San Diego mechanism with the addition of DME sub-mechanism, used in the simulations comprises 63 species and 284 reactions[2].

3.1.2 Other DME & Ethanol Mechanisms

One of the aforementioned mechanisms was developed by LLNL(Lawrence Livermore National Laboratory) is a dependable mechanism that has been proven across a wide range of parameters. This DME kinetic mechanism comprises of 251 reversible reactions and 49 species.

AramcoMech, a mechanism Developed by Curran et al., at NUI Galway. [13], is another very comprehensive mechanism. It is stated that a vast spectrum of experimental measures have been used to verify this mechanism. AramcoMech mechanism is a comparatively large mechanism with 766 reversible steps and 125 species.

Table 3.1. Table of DME sub-mechanism elementary reactions.

R#	Reaction
1	$CH_3OCH_3 \Leftrightarrow CH_3O + CH_3$
2	$CH_3OCH_3 + O_2 \Leftrightarrow CH_3OCH_2 + HO_2$
3	$CH_3OCH_3 + OH \Leftrightarrow CH_3OCH_2 + H_2O$
4	$CH_3OCH_3 + CH_3 \Leftrightarrow CH_3OCH_2 + CH_4$
5	$CH_3OCH_3 + H \Leftrightarrow CH_3OCH_2 + H_2$
6	$CH_3OCH_3 + HO_2 \Leftrightarrow CH_3OCH_2 + H_2O_2$
7	$CH_3OCH_2 \Leftrightarrow CH_2O + CH_3$
8	$CH_3OCH_2 + O_2 \Leftrightarrow CH_2O + CH_2O + OH$
9	$CH_3OCH_2 + O_2 \Leftrightarrow CH_3OCH_2O_2$
10	$CH_3OCH_2O_2 + CH_3OCH_2O_2 \Leftrightarrow O_2 + 2CH_3O + 2CH_2O$
11	$CH_3OCH_2O_2 \Leftrightarrow CH_2OCH_2O_2H$
12	$CH_2OCH_2O_2H \Leftrightarrow CH_2O + CH_2O + OH$
13	$CH_2OCH_2O_2H + O_2 \Leftrightarrow HO_2CH_2OCHO + OH$
14	$HO_2CH_2OCHO \Leftrightarrow CH_2O + CO_2 + OH + H$

Chapter 4

Numerical Simulation and Experiment

This section describes the experiments and computational investigations carried out for research studies. The Damköhler number, which was covered in the preceding sections, is a key parameter in combustion investigations. The followed procedure in the experiments and computational simulations is about controlling the Damköhler number. Oxidizer strain rate is used to control the Dahmköhler number. It is discussed in the section about Dahmköhler number, the increasing strain rate could decrease mixing and transport time so that Dahmköhler number could be decreased.

4.1 Experimental Setup

The main equipment of the experiment setup is the counter flow burner beside with fuel delivery system and oxidizer delivery system. Additionally, in order to improve the precision of experiment, a command software called LabView is used to control the experiment. This program allows for the recording of all input and output data as well as the calibration of mass flow controllers. One may view the real-time experiment data due to its graphical user interface. The counterflow configuration's schematic illustration was described in prior sections. To decrease the influence of ambient air on the reactive field, the fuel and oxidizer nozzles are concentrically positioned and surrounded by annular ducts. Thermocouples of the $R-type(Pt/13\%RhPt)$ were utilized in the tests. The cumulative uncertainty of the measurements with the $R-type$

thermocouples are accurate within $\pm 50K$. The intrinsic accuracy of $R-type$ thermocouples is considered when evaluating the uncertainty. A slight vacuum is created in the combustion zone that draws the combustion gases out without affecting the flame. The experiment setup also includes a water cooling system to aid in reducing the exhaust gases' reactivity prior to their release into exhaust system.

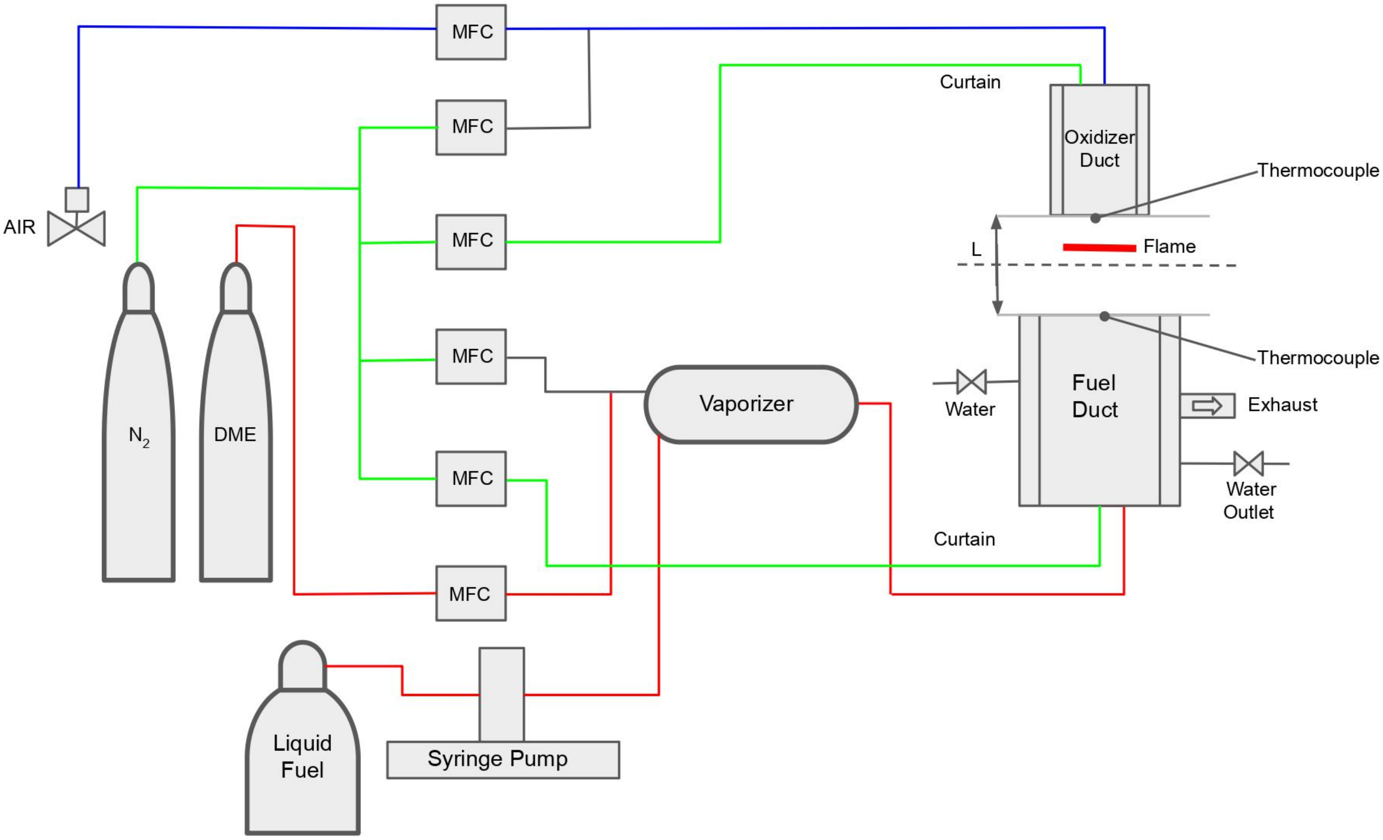

Figure 4.1. The experimental setup equipped with a counter flow burner is depicted schematically.

Previous research conducted by Prof. Seshadri's group at the University of California, San Diego, where the burner was designed, has in depth details and information regarding its design (e.g. [14][15].)

4.2 Experiments

Autoignition and extinction experiments were performed by Prof. Seshadri's group at the University of California, San Diego[1]. The fuel delivery(supply) mechanism for ethanol and dimethyl ether in the experiments operates as follows. Ethanol is provided via a syringe pump that is connected to the vaporizer and supplied to the fuel duct as gas. Dimethyl ether is provided from high pressure container and also nitrogen, which is used for curtain flow. Air is supplied from the oxidizer nozzle as the oxidizer using an air delivery system.

4.2.1 Autoignition Experiments

During the autoignition experiments a certain mixture fraction is selected and the strain rate was maintained constant. Throughout the experiment the oxidizer stream's temperature is enhanced to monitor the autoignition's critical conditions. In order to capture correct autoignition temperature, a high-speed camera is placed up along the centerline, where the maximum temperatures are detected. In table 4.1 the fuel composition for all autoignition simulation studies can be seen. The autoignition experiments are carried out for a total of 7 distinct blends, starting from pure ethanol to pure dimethyl ether with an increase of 20 percent of the dimethyl ether mass fraction.

Table 4.1. Fuel composition for all autoignition simulation studies.

	$Y_{Ethanol}$	Y_{DME}
1	1,00	0,00
2	0,80	0,20
3	0,60	0,40
4	0,40	0,60
5	0,20	0,80
6	0,00	1,00

4.3 Cantera

Cantera is an open source software package of multiple tools for chemical kinetics, thermodynamics and transport processes problems developed at the California Institute of Technology. Some capabilities of Cantera are as follows; one-dimensional flames, multiphase chemical equilibrium, homogeneous and heterogeneous chemistry, reactor networks, reaction path diagrams and electrochemistry [3].

Fast and efficient algorithms in this object-oriented structured tool allow users to rapidly integrate thorough chemical thermo-kinetics and transport models into their computations. Also it is compatible with the widely used chemical kinetics software tool Chemkin.

Cantera offers a variety of user-friendly interfaces. It supports usage from Matlab and Pyhton, or applications developed in Fortran 90, C/C++ and it can be also used with commercial CFD packages(e.g. Fluent). Cantera is still under development, and new features are constantly being added.

The software may be used for a variety of purposes, including developing customized reacting-flow codes and obtaining answers to simple investigative queries due to its practicality and simplicity. Most important features of Cantera are the extensibility and customization. It is possible to perform simulations using your own kinetics models, transport models, or thermodynamic models. One can make reaction path diagrams and do simulation of multiphase fluids. The program has several applications in areas such as combustion, detonations, electrochemical energy, plasmas etc.

4.4 Numerical Simulation Studies

Autoignition simulation codes are developed using Cantera software. San Diego mechanism is used in the simulations as the chemical kinetic reaction mechanism for computational combustion studies. The kinetic modeling simulations are carried out for various DME/Ethanol mixtures, including pure dimethyl ether and pure ethanol. In order to analyze the reaction mechanisms numerical results, experimental results from the study of A. Loukou et al [1] are reproduced using Cantera software.

4.4.1 Formulation of Simulation(Calculations)

The calculation procedures of autoignition analyses are described according to the San Diego Mechanism.

4.4.1.1 Autoignition Simulations

Calculations for autoignition analysis start at a constant strain rate and with initial temperatures of the experiment conditions for fuel inlet and oxidizer inlet. The velocities of the inlets are calculated by following the San Diego Mechanism. The oxidizer inlet velocity is calculated using the equation 2.1. Thereafter the fuel velocity is calculated using the momentum balance equation 2.2. The mass flow rates will be computed and the initial counterflow diffusion flame conditions will be specified in order to obtain the first solution. The autoiginiton temperature is then sought after following these steps using an iterative loop. In each iteration, it is ensured that the momentum balance is satisfied. The iterations continue to increase the temperature of the oxidizer until the flame is autoignited. At least five alternative strain rates are analyzed in the numerical simulations for each composition of dimethyl ether and ethanol blends.

Calculations for the flame solutions are conducted under refined grid condition of the Cantera software. Cantera has used between 60 and 90 grid points for the calculations at low strain rate and for the high strain rate calculations between 100 and 120 grid points are used.

Chapter 5

Results and Discussion

In the following sections one can see figures and plots discussing and comparing the simulation data and the experimental data from the study of A. Loukou et al [1].

5.1 Numerical Simulation Results compared with Experiments Data

Numerical simulation studies are performed for autoignition of mixtures of ethanol and dimethyl ether. For the autoignition experiments the conditions were as follows; fuel stream exit temperature was $400K(\pm 20K)$, the fuel mass fraction was $Y_{F,1} = 0.40$, and the duct separation was $L = 14.5mm$. For oxidizer, air was used, so the mass fraction for oxidizer was $Y_{O_2,2} = 0.233$. Autoignition experiments were performed by increasing the boundary temperature of the oxidizer T_2 until autoignition is occurred at a fixed strain rate, a_2. During experiments the adjustment of the velocities of the oxidizer and fuel flow has been done to keep the momentum balanced.

The experiment process was performed for various mixtures of dimethyl ether and ethanol as well as on various strain rate, a_2 values.

These studies investigated a variety of DME/ethanol blends, starting with pure ethanol and progressively enhancing the mass fraction of DME in the mixture by 0.20 up to pure DME, whereas the fuel mass fraction $Y_{F,1}$ was held constant at 0.40. Table 4.1 displays the tested blends. The measurements in the experiments were made utilizing the counter flow burner method.

The objective of the present work was to provide numerical simulation results from diffusion flames of DME and ethanol mixtures. Heat release rate analyses and reaction rate analyses are made at the heat release rate peak grid locations for all of the mixtures. As will be discussed in the following sections, certain mixtures had multiple peaks. Every peak in the mixture is therefore examined at its corresponding grid point location. The number of reactions to include in the heat release studies is determined based on how much of the total heat release the selected reactions contribute. It is not necessary to check the contribution of all reactions. Therefore, the cutoff percentage is picked as $\%80$. Only the contribution of reactions for heat release in the top $\%80$ is taken into analysis. The quantity limit for dominant reactions is thus set as ten reactions for the analyses.

5.1.1 Autoignition Results

One can observe the overall results of the autoignition temperature values in Figure 5.1. It can be seen that at low strain rates, $\%100$ ETH has the highest autoignition temperature and at high strain rates, $\%100$ DME has the highest autoignition temperature. The temperature of autoignition rises as DME content in the mixture increases. Detailed information about the results will be discussed in the following sections.

Low strain rate and high strain rate autoignition analyses are separated to perform autoignition analyses. The simulations are carried out at a constant pressure of $1atm$. Low strain rate simulations are performed at a value of $82.78s^{-1}$, while high strain rate simulations are run at a value of $246.78s^{-1}$, which are the values from the experimental data in the research of A. Loukou et al [1]. Heat release and autoignition temperature have the following relation. The temperature required for autoignition will be lower if the fuel's heat release is higher. Therefore, it is not needed to reach high temperatures for ignition in order to provide more heat to ignite the fuel. In other words, if the fuel itself releases enough heat, it is not needed to achieve high temperature for ignition. The importance of heat release analyses are to examine the relation between heat release and autoignition temperature. Knowing which reaction is dominant at the

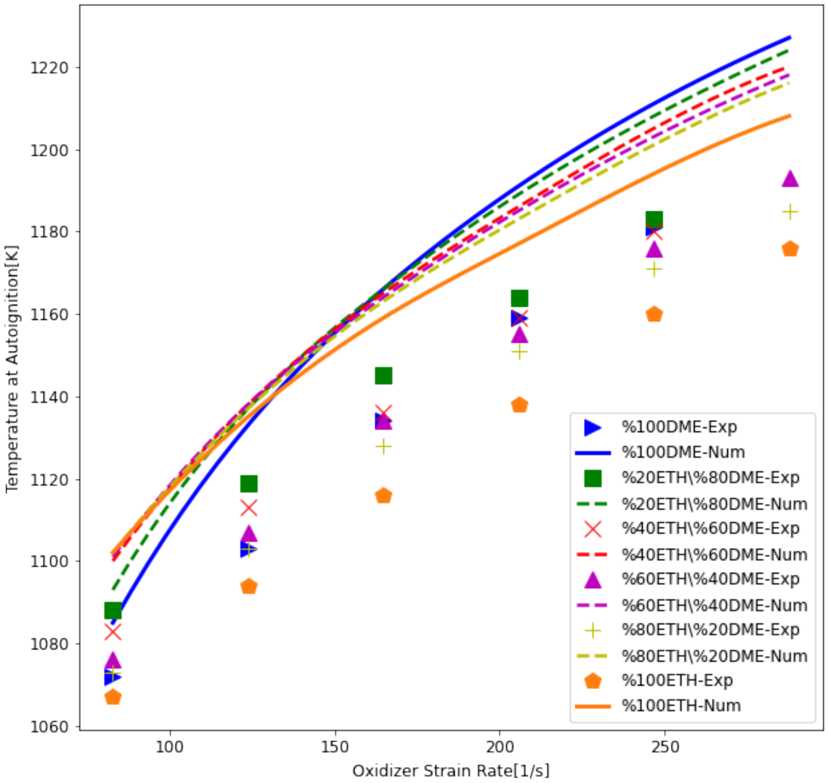

Figure 5.1. Autoignition temperatures of different mixtures from pure Ethanol to pure DME as a function of oxidizer strain rate.

onset of autoignition is beneficial for combustion studies. Figure 5.1 shows the autoignition temperatures as a function of the oxidizer strain rate for the computational simulation results and experimental data. In the numerical simulation results one can observe in figure 5.1 that at low strain rate value, pure ethanol has higher autoignition temperature than pure DME. On the other side it can be seen in figure 5.2 that pure ethanol has lower heat release value than pure DME. In figure 5.1 for autoignition temperatures at high strain rate, we observe that pure ethanol has lower autoignition temperature than pure DME, conversely for pure DME we observe higher autoiginition temperature. When comparing the heat release values, it can be seen that pure ethanol has higher heat release and pure DME has lower heat release. The results indicate that the obtained numerical simulation outcomes are consistent with the aforementioned relation about heat release and autoigniton temperature. In the next two sections, the causes of these combustion characteristics will be examined.

5.1.1.1 Low Strain Rate Autoignition Results

The San Diego Mechanism including the dimethyl ether(DME) sub-mechanism, comprises 284 reactions. The reactions of the San Diego Mechanism with the DME sub-mechanism implemented can be found in table 1 at Appendix A. The heat release analyses of dominant reactions are carried out, to determine which reaction is more potent on a given mixture. In addition, to comprehend which reactions are responsible for the heat release peaks. Also specifically, the causes behind the reactions to be dominant are investigated. The reasons could be the reaction rate of the dominating reaction, either forward or reverse, or the concentration of the reactants and products. Detailed reaction rate simulation studies are conducted to find the causes.

Low strain rate studies are performed at a strain rate value of $82.78s^{-1}$ and at a temperature of $1000K$. The analyses about the low strain rate autoignition results are starting with total heat release analyses. Figure 5.2 illustrates the comparison between the heat release of pure ethanol and the heat release of pure DME, which shows a single heat release peak for pure DME and three heat release peaks for pure ethanol, one negative heat release peak and two positive heat release peaks. Additionally, one can see that the magnitude of maximal heat release of pure ethanol is 10^{-4} times lower compared to the magnitude of maximal heat release of pure DME. $\%100$ ethanol has a maximum heat release rate value of $115\frac{W}{m^3}$, whereas $\%100$ DME has a maximum total heat release rate value of $6.8\times 10^6\frac{W}{m^3}$. Further analyses are conducted to study the combustion characteristics of the mixtures.

There is no flame showing in the reactive field and the temperature profiles throughout the whole grid are similar as depicted in figure 5.3. From the temperature profiles of the blends in figure 5.3 and from the heat release plots in figure 5.2, it can be stated that the peak of heat release of pure DME is shown to have occurred at $750K$ and the temperatures where the peak of

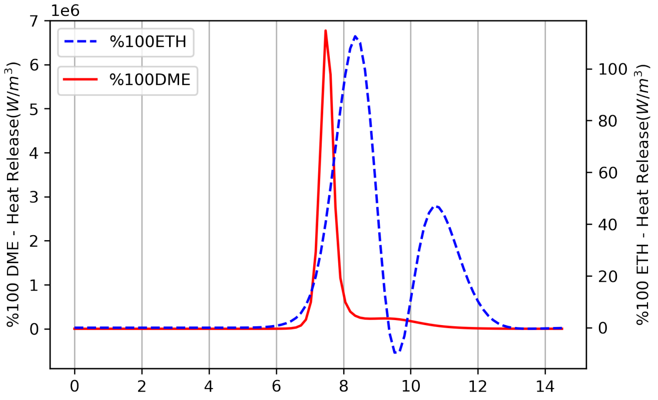

Figure 5.2. Total heat release values of %100 DME and %100 Ethanol blends over all grid points for low strain rate.

heat releases occur of pure ethanol are at 850K, 950K and 985K.

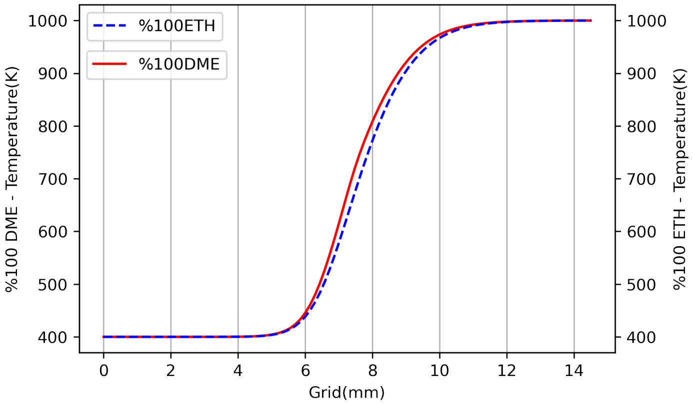

Figure 5.3. Temperature values of %100 DME and %100 Ethanol blends over all grid points for low strain rate.

The mass fraction decrease of the fuels DME and ethanol is proportionate when comparing the boundary values and the inner mass fraction values of the fuels while the transition from pure DME to pure ethanol is discussed, as illustrated in figure 5.4.

From %100 DME to %100 Ethanol there is an evolution of a high temperature heat release peak. Figure 5.5 shows the development of the high temperature heat release peak with the raise of ethanol in the blend. Also the heat release value is decreasing when the blend's ethanol content rises. The causes of the high temperature heat release peak's growth is examined. For each mixture, dominant reactions that had a role in the peaks of heat release are investigated.

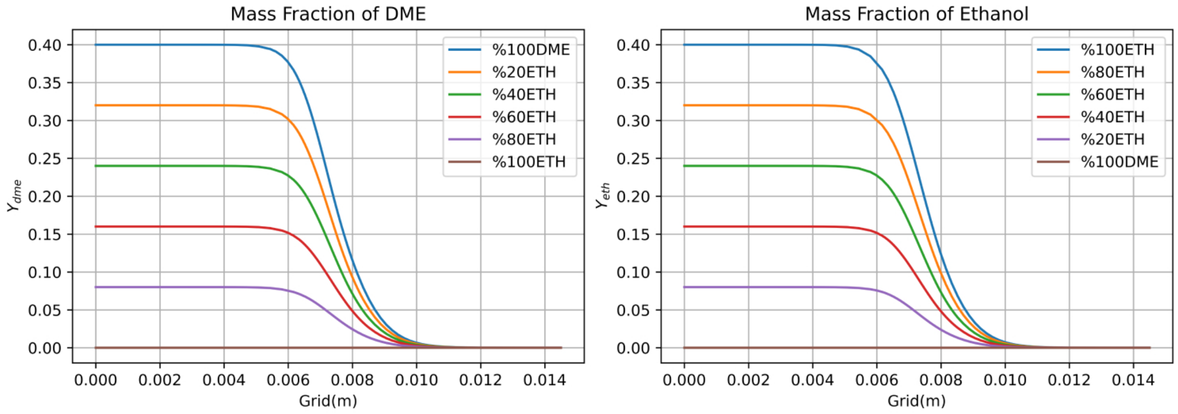

Figure 5.4. Left: DME Mass Fraction over all grid values of all mixtures. Right: Ethanol Mass Fraction over all grid values of all mixtures.

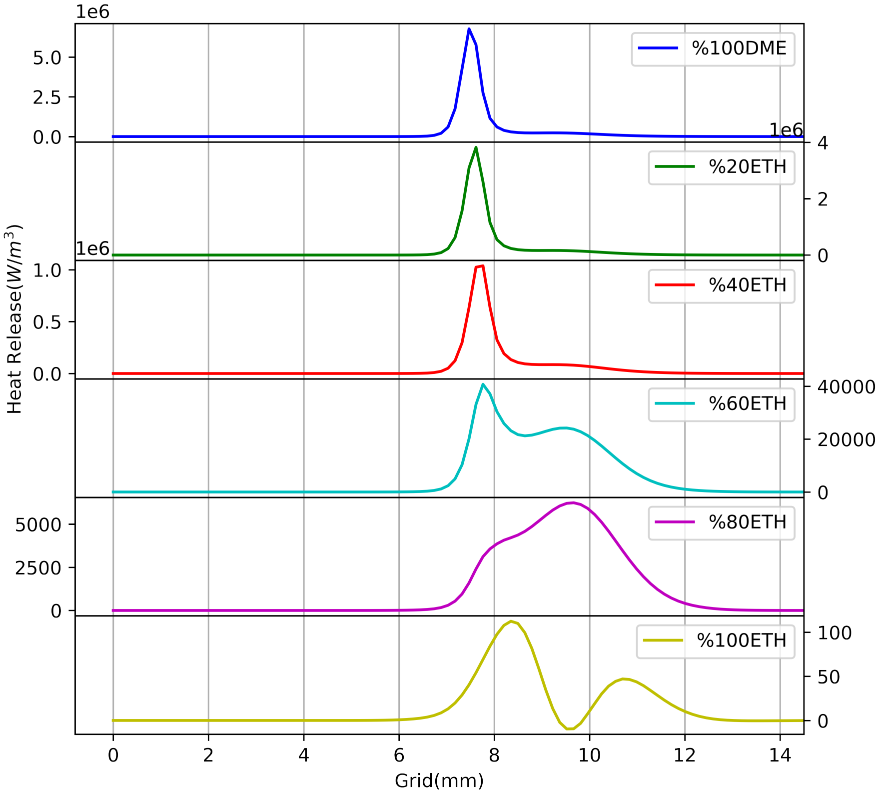

Figure 5.5. Second heat release peak value evaluation with the addition of ethanol to the mixture for low strain rate.

On figure 5.6, it can be seen that the total heat release value is decreasing with the addition of ethanol to the mixture. The most prevalent leading reaction of positive heat release for %100DME, %80DME-%20Ethanol and %60DME-%40Ethanol is reaction $R279 : CH_3OCH_2 + O_2 => CH_3OCH_2O_2$. The influence of this reaction, which comes from the DME sub-mechanism, is waning while still being the most influential as the ethanol level rises in the mixtures %80DME-%20Ethanol and %60DME-%40Ethanol. Moreover $R273 : CH_3OCH_3 + OH <=> CH3_3OCH_2 + H_2O$ and $R282 : CH_2OCH_2O2H <=> CH_2O + CH_2O + OH$ are dominant reactions of the positive heat release data. $R281 : CH_3OCH_2O_2 <=> CH_2OCH_2O_2H$ is the reaction that dominates when the negative heat release is taken into account. Reaction rate figure 5.7, shows that in line with the aforementioned statement about the dominance of the reactions, the highest reaction rates for the blends %100 DME, %80DME-%20Ethanol and

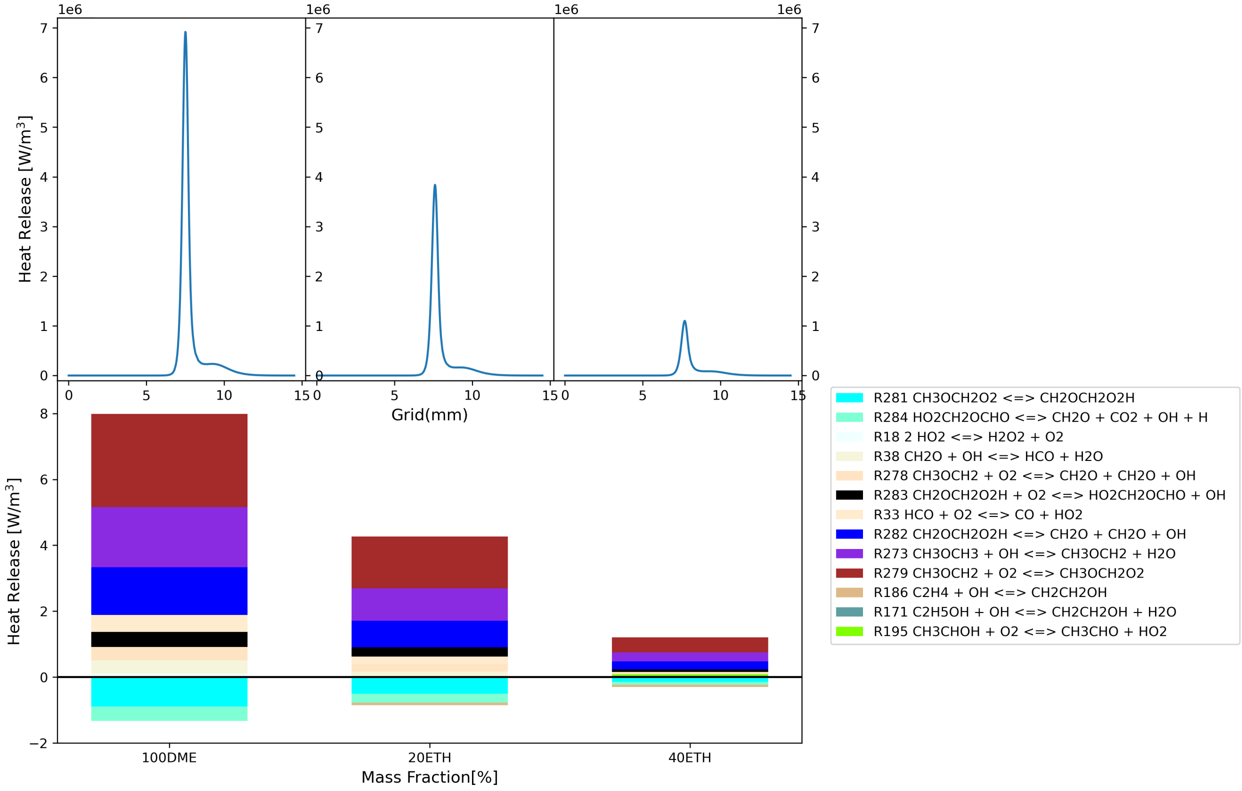

Figure 5.6. Heat release and dominant reactions shown in each mixture for %60 DME-%40 ETH %80-%20 ETH DME and %100 DME for low strain rate.

%60DME-%40Ethanol are $R279$, $R273$ and $R282$. Similar to the decrease in the heat release maximal values while Ethanol is added to pure DME, the reaction rate maximal values are decreasing. For reactions R279 and R282, the forward reaction rate is dominant but the forward reaction rate constant is steady, nearly identical for the reactions. Further investigations indicate that the concentrations of the reactants, CH_3OCH_2 and $CH_2OCH_2O_2H$, are reducing which explains why the reaction rate value is declining as can be seen in figure 5.7. Comparison of the three mixtures reveals, reaction R273 has the highest reaction rate. The reactants of R273 are CH_3OCH_3 and OH. It can be seen that the forward rate of the reaction is dominant to the reverse rate from figure 5.7. The analyses show that the forward reaction rate constant for reaction R273 remains nearly steady. The primary reason of the decrease of the reaction rate is with the decrease of the inlet mass fraction of CH_3OCH_3.

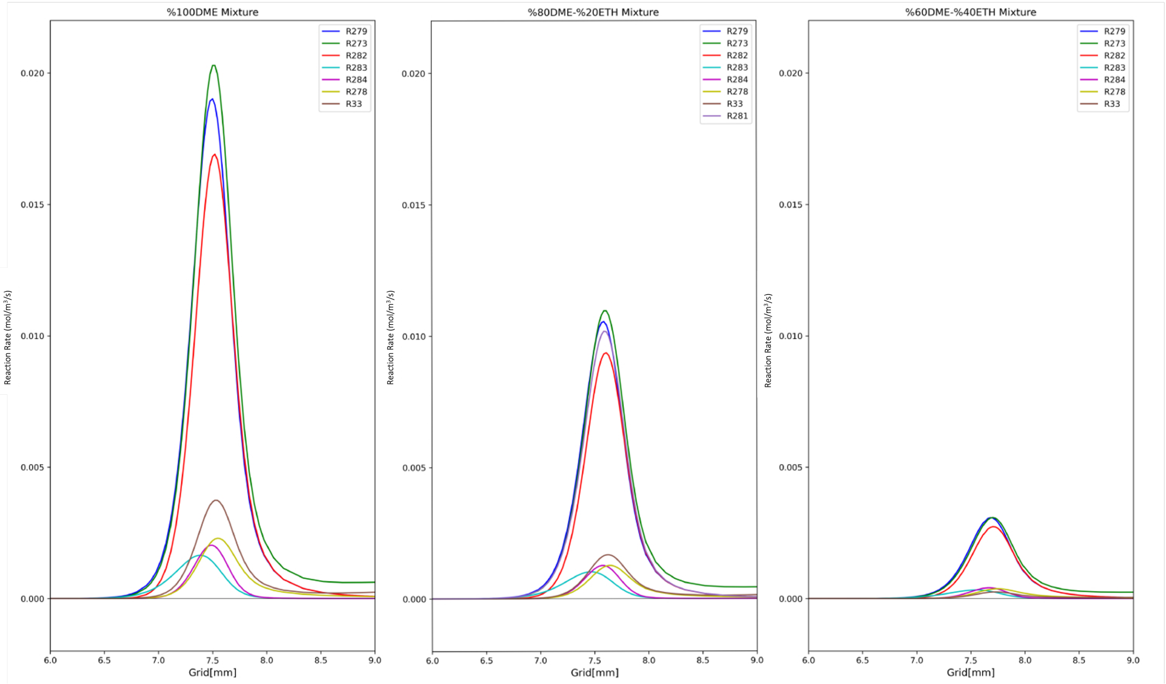

Figure 5.7. Left: %100DME Reaction Rate Values for low strain rate. Middle: %80 DME-%20 ETH Reaction Rate Values for low strain rate. Right:%60 DME-%40 ETH Reaction Rate Values for low strain rate.

All important reactions related to DME in heat release are shown in figure 5.8. In fact, the decrease in inlet mass fraction of DME causes a chain effect of important reactions in heat

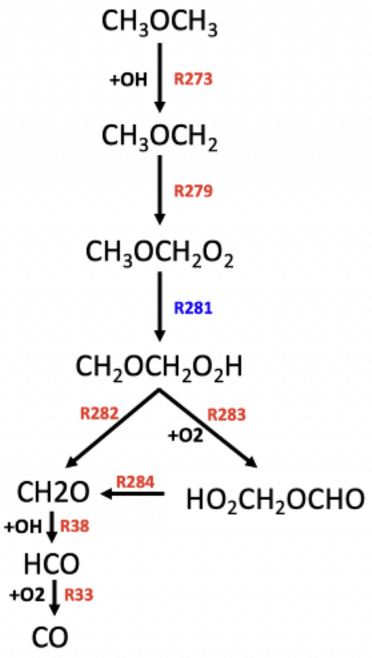

Figure 5.8. Important reactions in heat release related with dimethyl ether.

release and most of them cause positive influence in heat release. Therefore, when the mixture is changing from %100DME to mixtures with more ethanol, decline in DME percentage causes the heat release decrease. Additionally, there is competition for OH species between ethanol and DME at the initial DME reactions stage(R273). When ethanol is added to the mixture, OH is also consumed with C_2H_5OH in reactions R171 and R173. These reactions are getting more dominant as ethanol percentage in the mixture is increased. Reaction rate analyses indicate that the forward reaction rate constants of the reactions R171 and R173 are increasing and also the concentration of ethanol species is increasing, therefore their reaction rates are increasing. Since both DME reactions and ethanol reactions are using OH as reactant, the addition of ethanol to the mixture causes a competition which results with a decrease of dominance of DME related reactions. The net reaction rate values of OH related dominant reactions for the mixtures %100 DME, %80 DME-%20 ETH and %60 DME-%40 ETH are shown in the bar graphs in figure 5.9. As can be observed from figure 5.9 the reactions R171 and R173 start to be more dominant as ethanol is added to the mixture.

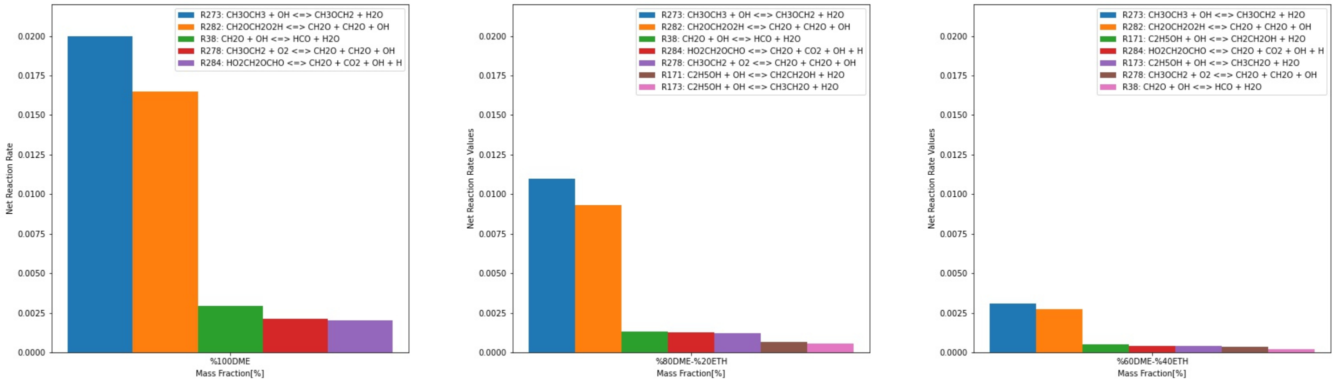

Figure 5.9. Net reaction rate values for *OH* related dominant reactions of %100 DME, %80 DME-%20 ETH and %60 DME-%40 ETH mixtures for low strain rate.

In Figure 5.5 one can start to observe the second heat release rate peak clearly at the mixture %60 Ethanol-%40 DME. The heat release rate bar graphs of %60 Ethanol-%40 DME and %80 Ethanol-%20 DME are shown in figure 5.10. When comparing these two mixtures, it can be seen that the maximal heat release rate value is decreasing and in the meantime at %60 Ethanol-%40 DME the total heat release rate value of the low temperature heat release peak is higher than the high temperature heat release peak but for %80 Ethanol-%20 DME the maximal heat release rate value of the high temperature heat release peak is greater than the low temperature heat release peak. As depicted in figure 5.10, one can see that R279 is still the most dominant reaction for the low temperature heat release peak in %60 Ethanol-%40 DME but for %80 Ethanol-%20 DME it loses its dominance since it is a reaction from the sub-mechanism of DME and its influence is waning as the DME proportion in the blend lessens. R282 is also one of the reactions that dominates %60 Ethanol-%40 DME, but when the DME content goes from %40 to %20, its dominance also diminish. For the reactions which have negative effect on heat release, one can still see R186 and R281 as dominant reactions for the low temperature heat release peak. One begins to witness R277 and R16 in addition to R186 as high temperature heat release peak dominating reactions on the negative heat release. Reaction rate plots of the mixtures at figure 5.11 gives further explanation about the double peaked graphs. Figure 5.11

shows that R279 is a reaction that influences the low temperature heat release peak since the reaction rate peak of R279 is also located at the same grid position. R282 has a similar effect like R279, from figure 5.11 one can see that the reaction rate values of these reactions are getting ten times smaller. Reaction rate analysis about R279 shows that the forward reaction rate remains constant but the concentration of its reactant CH_3OCH_2 is decreasing so the reaction rate is decreasing. For R282, the forward reaction rate constant remains nearly same compared to the drop in its reactants $CH_2OCH_2O_2H$ concentration. R52's reaction rate peak is located at high temperature heat release peak and therefore has high influence on the high temperature heat release peak as can bee seen in the reaction rate graph in figure 5.11. The reaction rates of DME reactions, R279, R282 and R281, which are influencing the low temperature heat release peak are declining rapidly compared to R52. So, in the %20 DME-%80 ETH mixture one can observe that the high temperature heat release peak maximal value is exceeding the low temperature

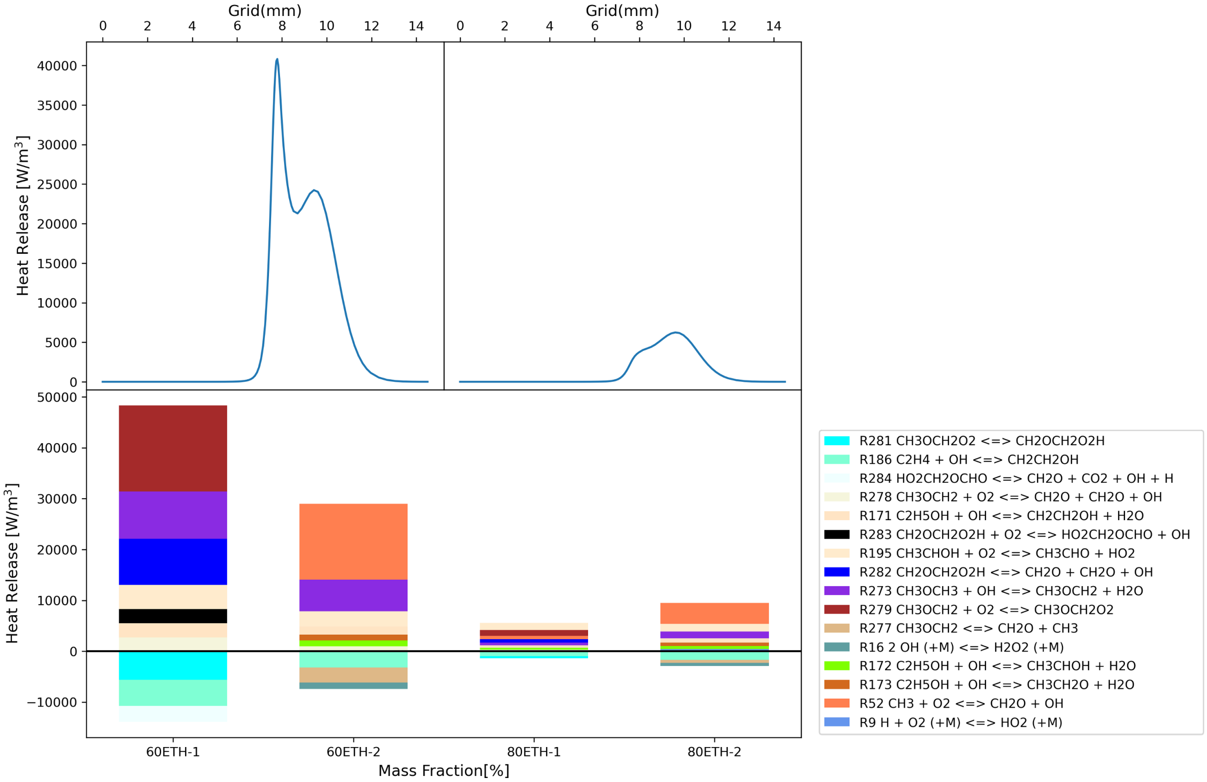

Figure 5.10. Heat release and dominant reactions shown in each mixture for %60 ETH-%40 DME and %80 ETH-%20 DME for low strain rate.

heat release peak maximal value. For reaction R186 one can observe negative reaction rates for both of the mixtures, moreover at %60 Ethanol-%40 DME it influences the low temperature heat release peak but at %80 Ethanol-%20 DME its influence is more effective on the high temperature heat release peak. The reaction rate of R186 for low temperature heat release peak is decreasing more than the high temperature heat release peak. Further investigations show that, on the low temperature heat release peak show that the forward reaction rate constant of R186 and its reactants, C_2H_4 and OH, are decreasing more rapidly compared to the high temperature heat release peak which contributes to the reduction in net reaction rate.

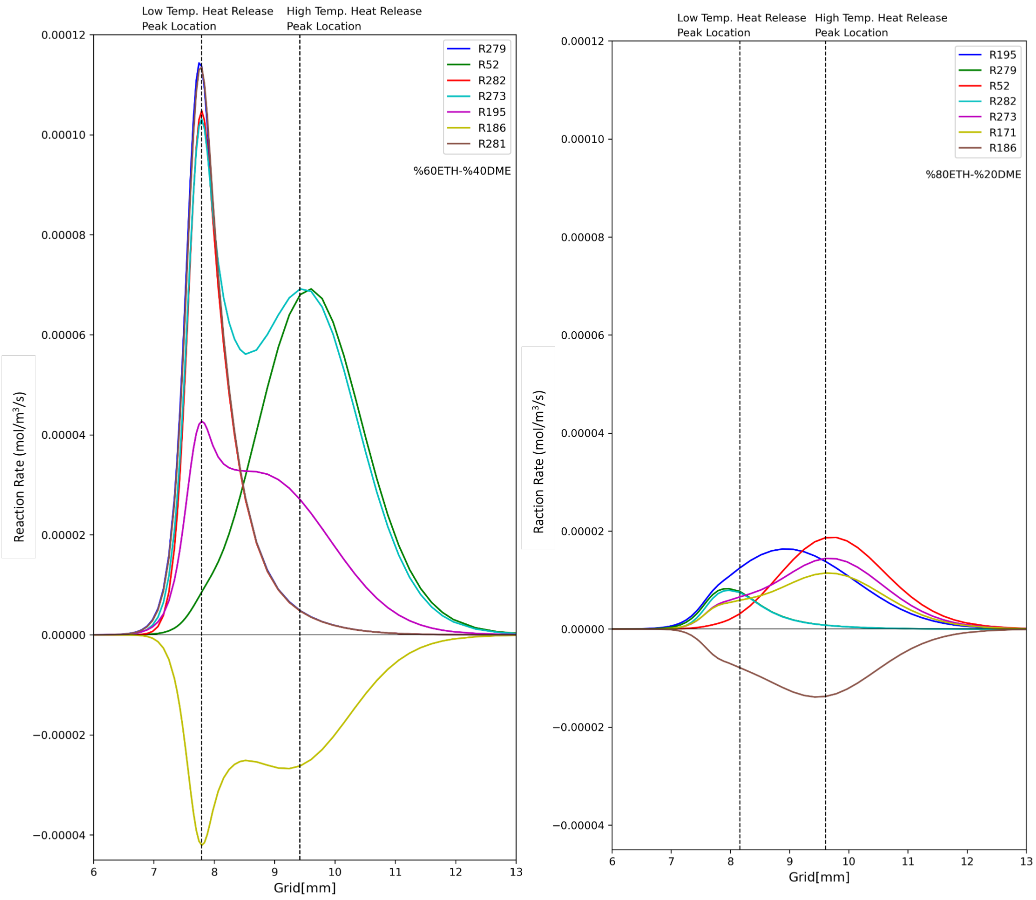

Figure 5.11. Left: %40 DME-%60 Ethanol Reaction Rate Values for low strain rate. Right: %20 DME-%80 Ethanol Reaction Rate Values for low strain rate.

Pure ethanol heat release rate graphic has three peaks as shown in figure 5.12. Beside R52, which had started to be dominant with the increase of ethanol content in the mixture, R195 and R171 have a positive dominant effect among the three heat release peaks. Since the intermediate temperature heat release peak is below zero, the magnitude of sum of the negative heat release values is larger than the magnitude of sum of the positive heat release values. At the low temperature heat release peak location, dominant reaction for negative heat release is R183, different from the high temperature heat release peak and intermediate temperature heat release peak. The dominant negative influence of high temperature heat release peak and intermediate temperature heat release peak come from R170, R186, R16 and R188. The reasons behind these situations are investigated using the reaction rate data in figure 5.13. The low temperature heat release peak location is named as first peak, the intermediate temperature heat release peak as second peak and the high temperature heat release peak is named as third peak in the figure 5.13. As can be seen in figure 5.13 R195's reaction rate peak is located between low temperature heat release peak and high temperature heat release peak, closer to the low temperature heat release peak. R170 has a relative higher reaction rate peak compared to other reactions, located at same location with high temperature heat release peak. The negative reaction rate curve for R186 is positioned at the high temperature heat release peak and has a significant impact on the other two peaks as mentioned in the heat release analysis. The moderate decline in the reaction rates of R195, R171 and R52, along with the steep decline of R170 and R186, aid in the formation of the third peak.

5.1.1.2 High Strain Rate Autoignition Results

All high strain rate analyses are conducted at $246.78s^{-1}$ and at a temperature of $1175K$. To begin with, figure 5.14 illustrates the comparison of the high strain rate heat release graphs of pure ethanol and pure DME. It can be seen in figure 5.14 that for high strain rate pure ethanol has one heat release rate peak and pure DME has two heat release rate peaks while at low strain rate analysis for pure DME two heat release peaks and for $\%100$ Ethanol one heat release peak was observed. Comparing the difference between pure ethanol and pure DME maximal heat release peak values, for high strain rate the magnitudes are in same order of magnitude but for low strain

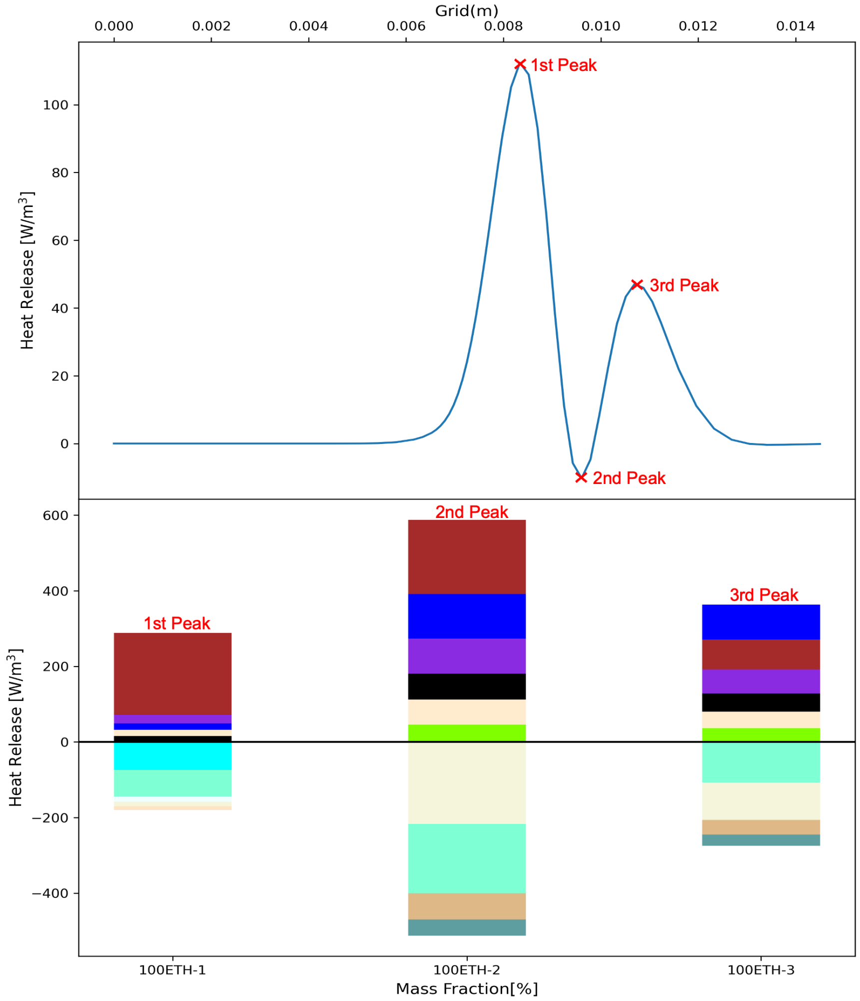

Figure 5.12. Heat release and dominant reactions shown in each mixture for %100 ETH for low strain rate.

rate the difference between the maximal magnitudes was quite large. Further investigations are conducted to comprehend the change in the behavior.

With the absence of a flame over the reactive field, the temperature profiles of the pure fuels are similar. From the temperature profiles of the fuels in Figure 5.15, the peak of heat release of pure DME is shown to have occurred at $750K$ and $1150K$. The temperatures where the peak of heat release occurs for pure ethanol is at $1150K$.

Figure 5.16 shows the evaluation of the low temperature heat release peak with the addition of DME. Also one can see the slight shift of the location of the low temperature heat

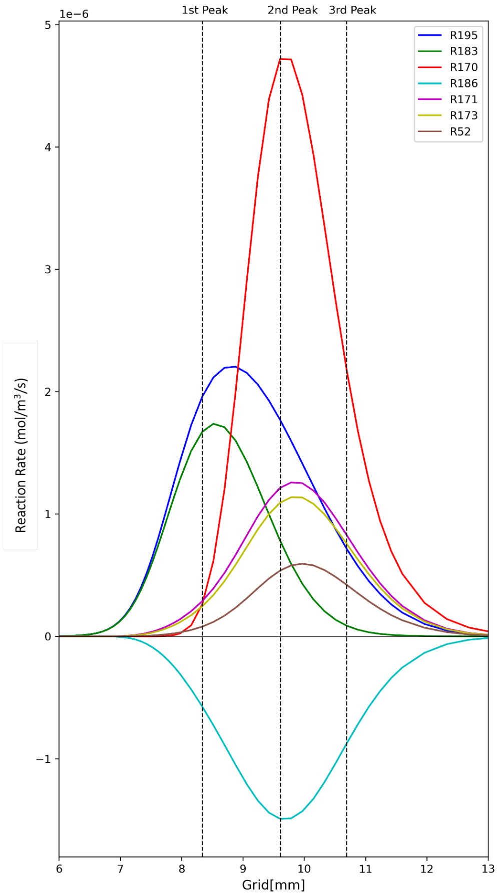

Figure 5.13. %100 ETH Reaction Rate Values for low strain rate.

release peak to the fuel side. A total comparison of all the heat release rate curves is also depicted in figure 5.16. As mentioned before it can be seen that they are in same order of magnitude. The evolution of low temperature heat release peak continues until the low heat release temperature peak at pure DME is becoming larger than high temperature heat release peak.

Heat release rate analyses of %100 Ethanol and %80 Ethanol-%20 DME mixtures can be seen in figure 5.17. The addition of DME to the mixture decreases the maximal heat release rate value. As soon as DME is added to the mixture, DME sub-mechanism reactions begin to appear in the dominant reactions. For both of the mixtures the first three dominant reactions, $R33 : HCO + O_2 <=> CO + HO_2$, $R38 : CH_2O + OH <=> HCO + H_2O$ and $R52 : CH_3 + O_2 <=> CH_2O + OH$ remain same. Forward reaction rates of these reactions are considerably larger

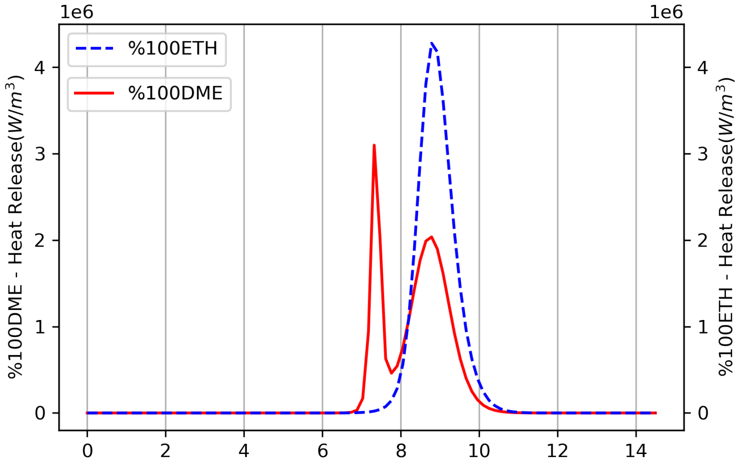

Figure 5.14. Total heat release values of %100 DME and %100 Ethanol blends over all grid points for high strain rate.

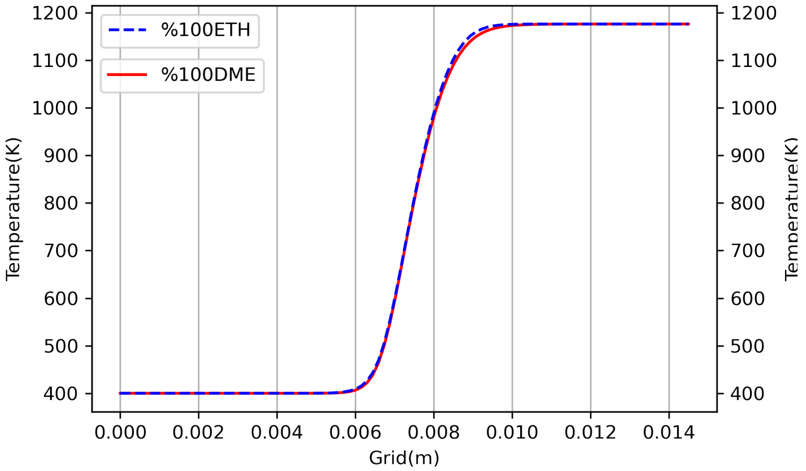

Figure 5.15. Temperature values of %100 DME and %100 Ethanol blends over all grid points for high strain rate.

than reverse reaction rates. Reaction $R171 : C_2H_5OH + OH <=> CH_2CH_2OH + H_2O$ which has ethanol species as reactant is also dominant for %100 Ethanol and %80 Ethanol-%20 DME. For the reactions which have negative effect on heat release, reaction $R186 : C_2H_4 + OH <=> CH_2CH_2OH$ and $R16 : 2OH(+M) <=> H_2O_2(+M)$ are dominant. From figure 5.18 one can observe that the reaction rate magnitudes are decreasing with the addition of DME. As can be

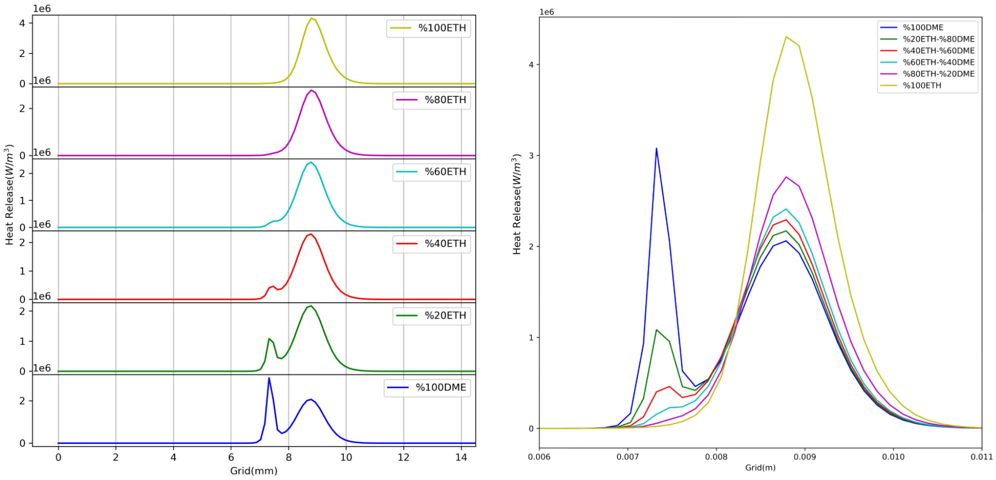

Figure 5.16. Second heat release peak value evaluation with the addition of ethanol to the mixture for high strain rate.

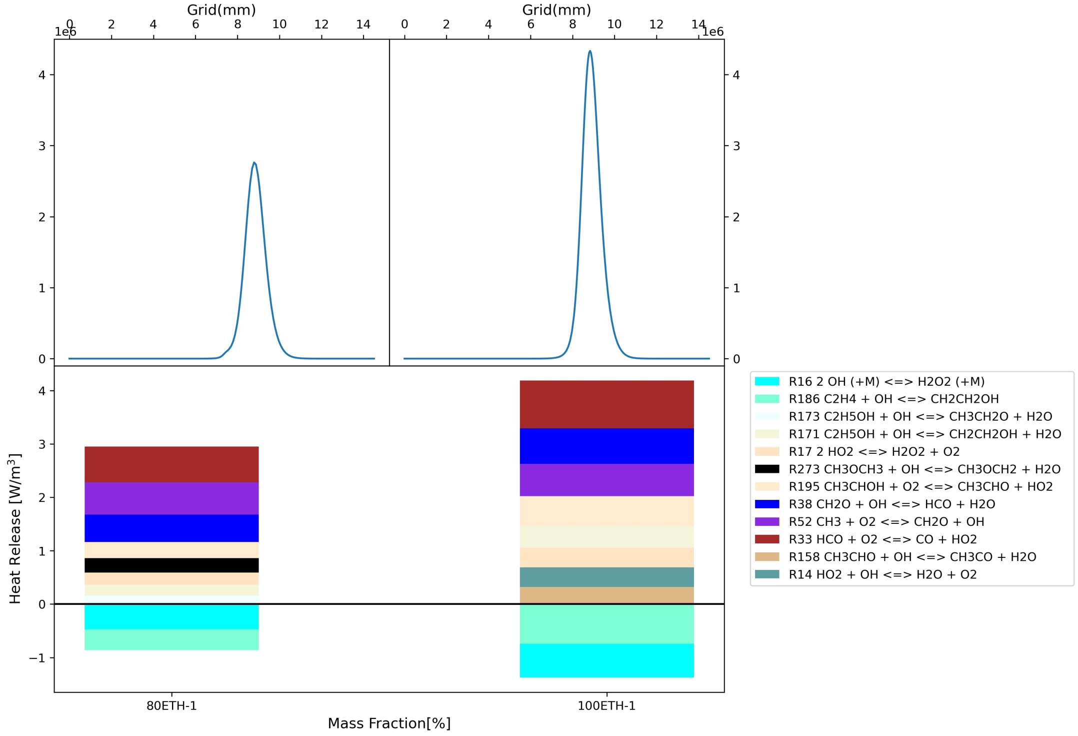

Figure 5.17. Heat release and dominant reactions shown in each mixture for %80 ETH-%20 DME and %100 ETH for high strain rate.

seen, R195 and R171 appear to be dropping down more swiftly than the other reactions. For R195, detailed analyses show that the forward reaction rate constant and the concentration of the reactant CH_3CHOH, is decreasing and the concentration of the other reactant O_2 stays constant, which results with a drop in the reaction rate. The reaction rate decline of R171 is explained with the slight decrease of the forward reaction rate constant and significant decrease of its reactant's concentration of OH.

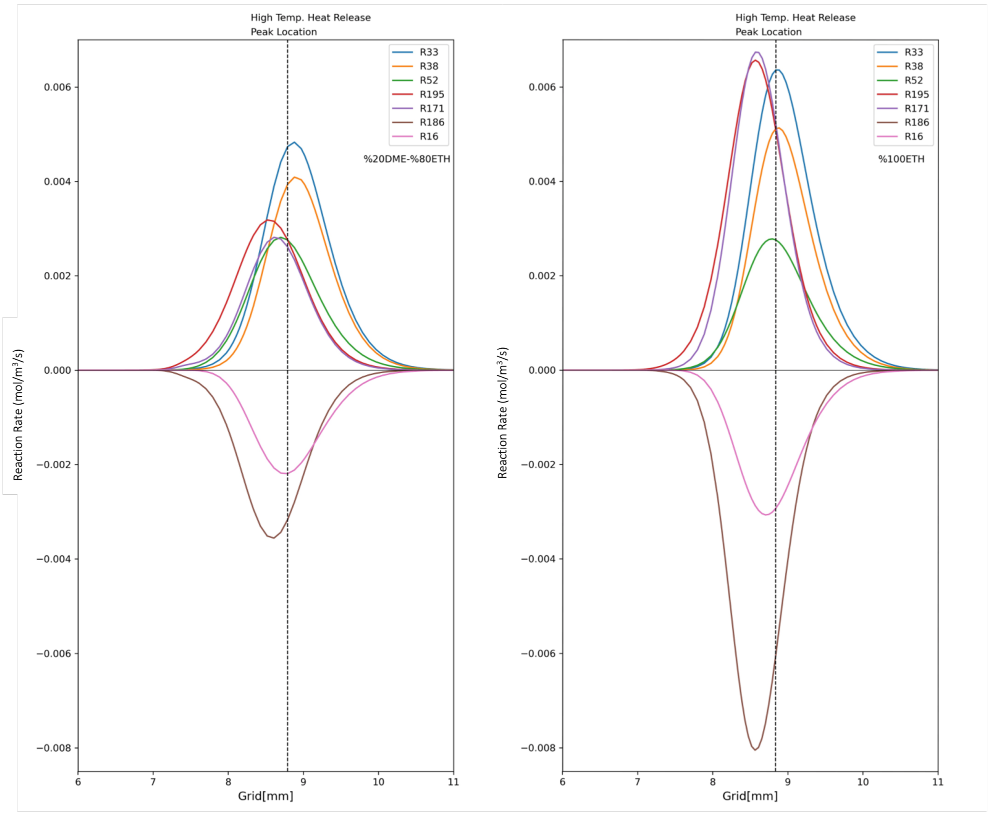

Figure 5.18. Left: %20 DME-%80 Ethanol Reaction Rate Values for high strain rate. Right: %100 Ethanol Reaction Rate Values for high strain rate.

The low temperature heat release peak appears when the concentration of DME in the mixture rises at %60 Ethanol-%40 DME as can be seen in figure 5.19. Dominant reactions of the high temperature heat release peak remain constant as R52, R33 and R38. But for the low temperature heat release peak the dominance is taken over by DME related reactions. And one start to see $R279 : CH_3OCH_2 + O_2 => CH_3OCH_2O_2$ and $R273 : CH3OCH3 + OH <=>$

$CH3OCH2 + H2O$ as dominant reactions for the low temperature heat release peak. As can be seen in figure 5.20, reaction $R277 : CH3OCH2 <=> CH2O + CH3$ which is a DME related reaction, has the highest reaction rate value. One start to see its influence one the high temperature heat release peak, since the reaction rate peak is also located close the high temperature heat release peak. For %40 Ethanol-%60 DME mixture, the low temperature heat release peak is more visible since the sum of individual reactions' heat release values for the low temperature heat release peak is higher. Also R17 and R195 are not displayed anymore in figure 5.20 which indicates that they are not dominant anymore according to the limit for dominance at high strain rate. In-depth analyses show that for R279 the reaction rate constants are remaining the same but the concentration of the reactant CH_3OCH_2, is increasing specially for the low temperature heat release peak. The low temperature heat release peak's growth is the most evident observation that can be made from figure 5.21. As DME increase from %80 to %100, low temperature heat

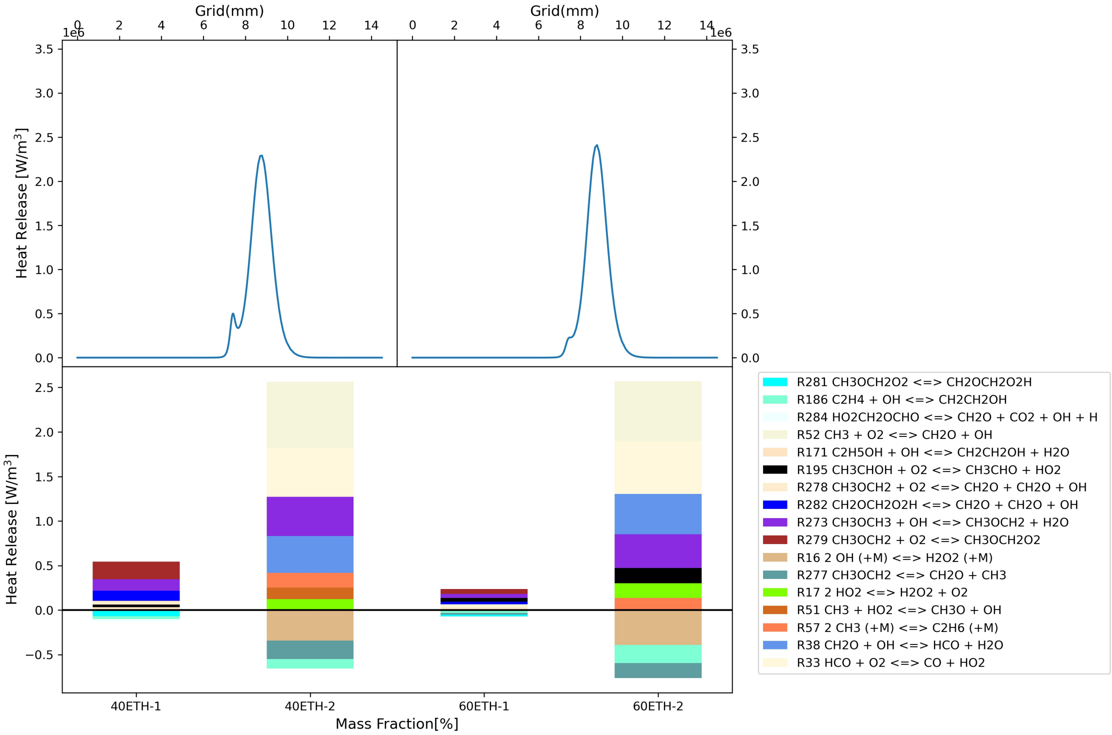

Figure 5.19. Heat release and dominant reactions shown in each mixture for %60 ETH-%40 DME and %40 ETH-%60 DME for high strain rate.

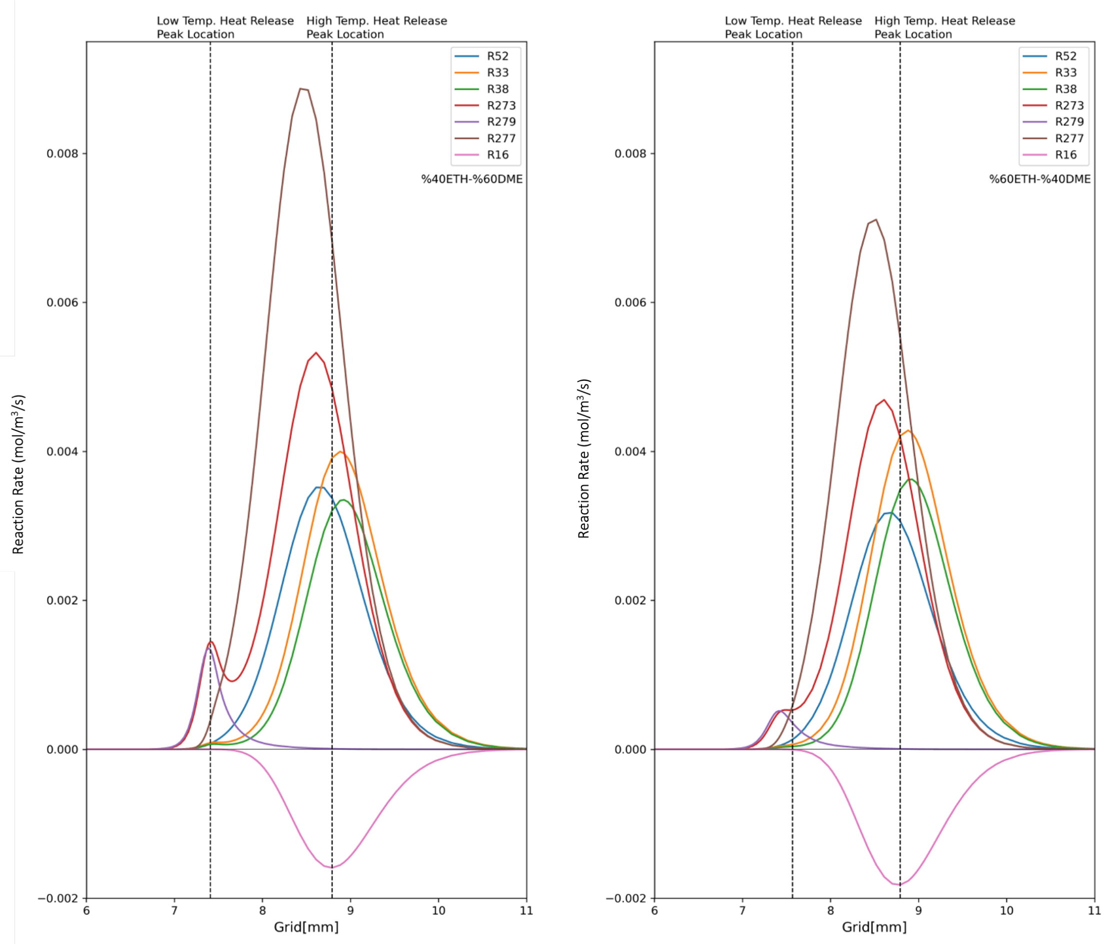

Figure 5.20. Left: %60 DME-%40 Ethanol Reaction Rate Values for high strain rate. Right: %40 DME-%60 Ethanol Reaction Rate Values for high strain rate.

release peak transcends the high temperature heat release peak because DME is responsible for the reactions of the low temperature heat release peak. On the path to pure DME, R279 eventually overtook all other reactions as the dominant reaction overall for the low temperature heat release peak. Also the net heat release rate values of low temperature heat release peak in pure DME is higher than the high temperature heat release peak. Another noteworthy feature is that R273 is dominant in both of the peaks of both mixtures. For reaction R277, the reaction rate is remaining nearly the same for the high temperature heat release peak but the reaction rate is increasing for the low temperature heat release peak as DME increases from %80 DME to %100 DME. The reaction rate analyses for high strain rate analyses can be seen in figure 5.22. At the low temperature heat release peak location for R279, the forward reaction rate constant and the concentration of O_2 is remaining same but the concentration of CH_3OCH_2 is increasing from %80DME-%20ETH to %100DME, therefore its dominance is increasing. For R273, the reaction rate constant is remaining nearly same but the concentration of both of the reactants, CH_3OCH_3 and OH, are increasing at low temperature heat release peak location.

At the low temperature heat release peak location, DME related reaction rates are increasing and ethanol related reaction rates are decreasing. From %80 DME to %100 DME at low temperature heat release peak location the concentration of OH is increasing. The increase in mass fraction of DME in inlet triggers a chain effect of dominant reactions in heat release. So, the increase of DME mass fraction is increasing the heat release peak value of low temperature heat release peak. Furthermore, when ethanol content is decreasing in the mixture, in the competition for OH the DME reactions become more important. In figure 5.23, a comparison of %60 DME-%40 ETH, %80 DME-%20 ETH and %100 DME mixtures for OH related reactions at low temperature heat release peak is prepared using the net reaction rate data. Figure 5.23 shows that the net reaction rates of the OH related ethanol reactions R171 and R173 are decreasing. Reactions R171 and R173 have C_2H_5OH and OH as reactants and are losing their dominance when DME is added to the mixture. The forward reaction rate constants of R171 and R173 are decreasing and also the concentration of C_2H_5OH is decreasing which causes to a drop in reaction rates which also can be seen in figure 5.23. At high temperature heat release peak location it is observed that R38, R52 and R33 are taking the top dominant roles in all mixtures. From pure ethanol to pure DME, dominance of R195, related to ethanol, is decreasing. Conversely, R273, related to DME, become more important with the addition of DME.

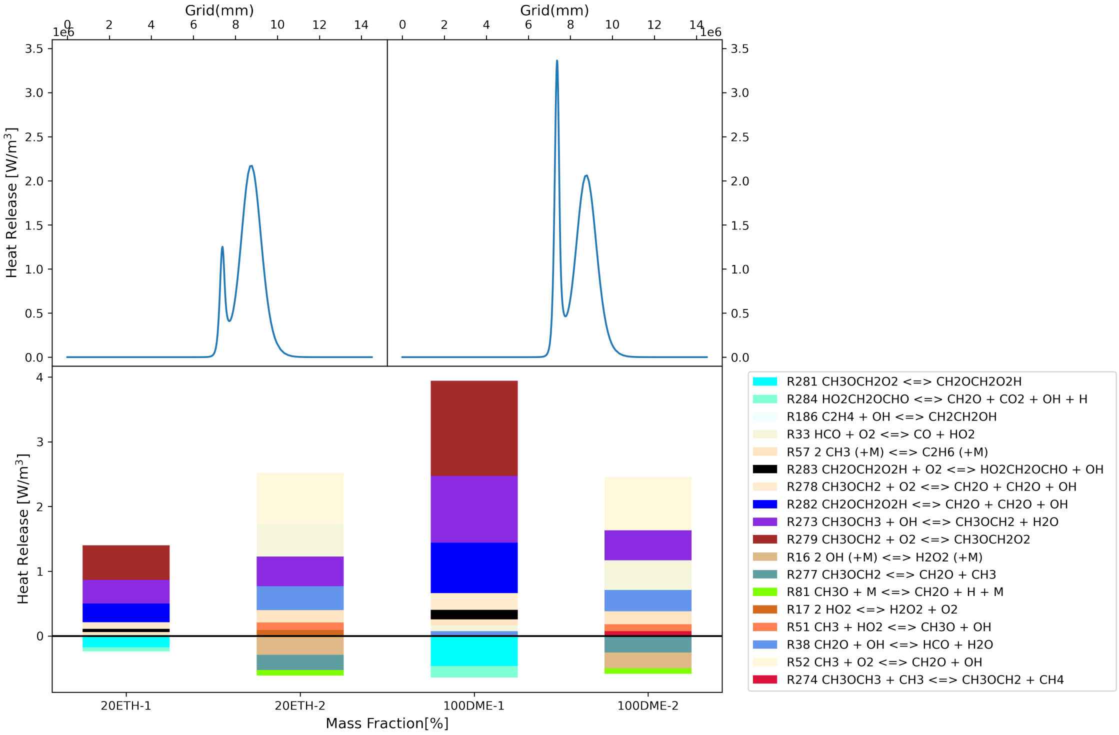

Figure 5.21. Heat release and dominant reactions shown in each mixture for %20 ETH-%80 DME and %100 DME for high strain rate.

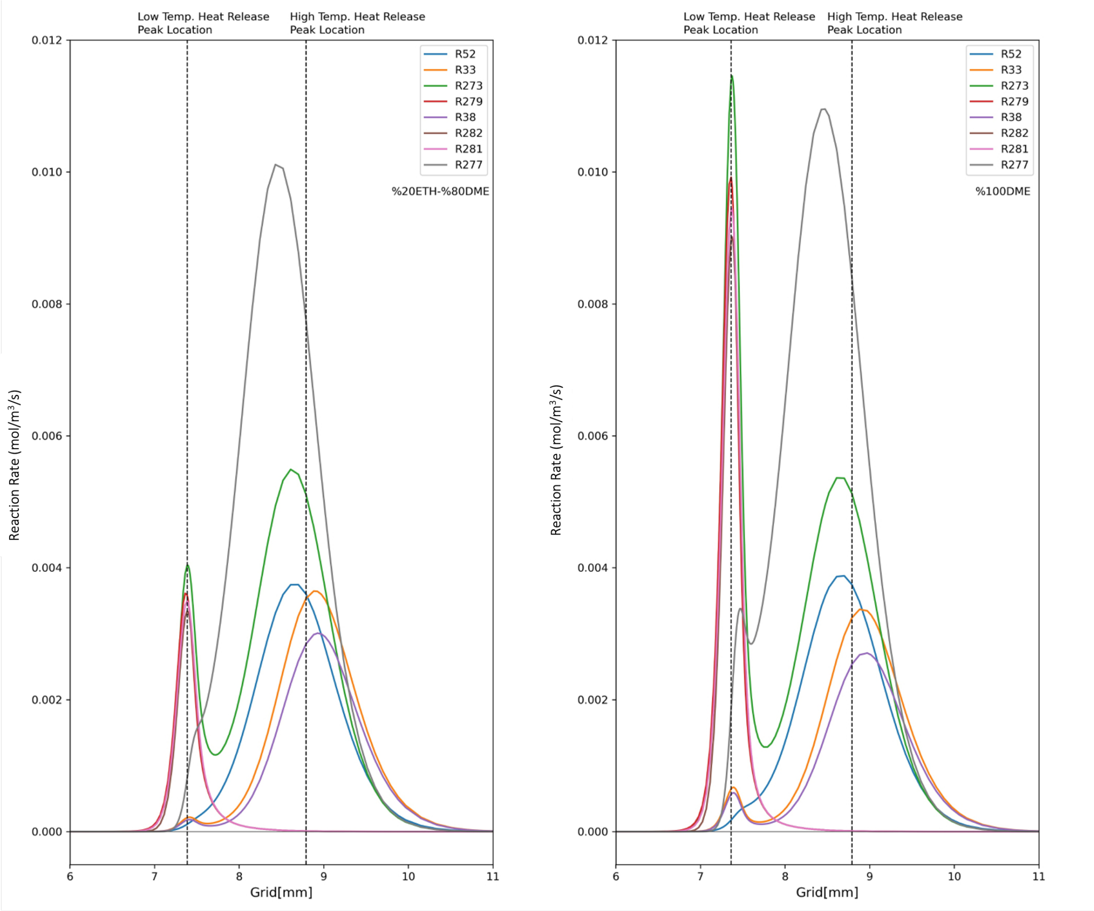

Figure 5.22. Left: %80 DME-%20 Ethanol Reaction Rate Values for high strain rate. Right: %100 DME Reaction Rate Values for high strain rate.

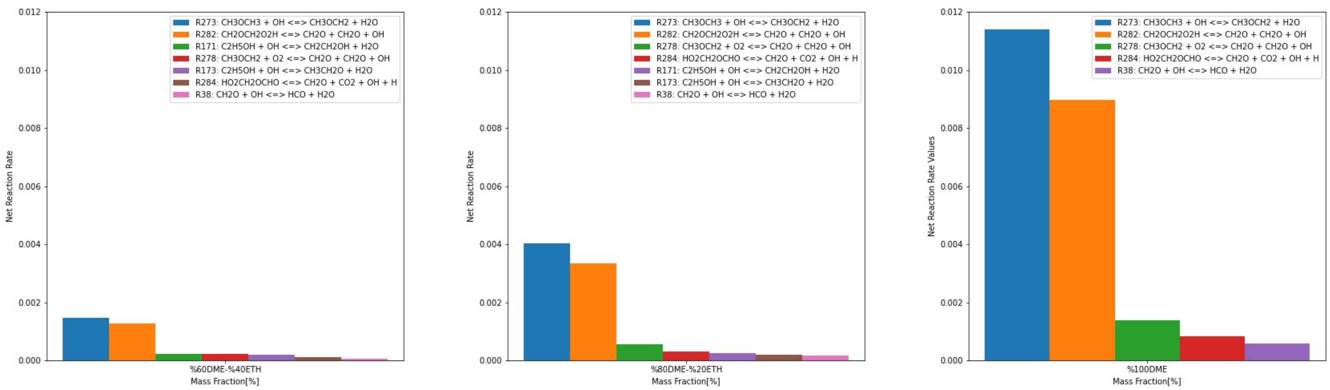

Figure 5.23. Net reaction rate values for *OH* related dominant reactions of %60 DME-%40 ETH, %80 DME-%20 ETH and %100 DME mixtures for high strain rate.

Chapter 6

Conclusion and Future Work

Numerical simulation studies were carried out using the San Diego mechanism developed by the combustion group at University of California San Diego. Detailed analyses on heat release rate revealed information about the dominance of the individual reactions. These analyses were used to elucidate the dominance spectrum of the reactions according to the change of the content of ethanol and dimethyl ether in the fuel mixture. Additionally, reaction rate analyses were conducted to determine the factors that influence the prevalence of the dominant reactions in the various dimethyl ether and ethanol mixtures.

As strain rate increases, autoignition temperatures of pure fuels also increase. Specifically for pure DME, the increase in autoignition temperature is higher than pure ethanol.

Low strain rate autoignition analyses have shown that pure DME has the lowest autoiginition temperature and the highest heat release peak value. The addition of ethanol to the mixture causes an increase in the autoignition temperature and a decrease in heat release peak value. Dominant reaction analyses showed that there is a chain of reactions related from CH_3OCH_3(DME) with OH. Hence, the heat release is impacted by the decline of the mass fraction of DME in inlet. Moreover, competition of OH species consumption by ethanol related reactions is increased while the ethanol content in the mixture is increasing. This enhances the dominance of OH related ethanol reactions.

Similar characteristics to low strain rate reactions are observed in the high strain rate analyses for the low temperature heat release peak value. From pure ethanol to pure DME, dominance of the chain of reactions from CH_3OCH_3(DME) to OH increases while the competition for OH species between ethanol and DME decreases. According to high strain rate autoignition investigations, pure ethanol has the lowest autoignition temperature and the highest heat release peak value. As DME is added to the mixture, the temperature required for autoignition increases and heat release peak value decreases. At high temperature heat release peak value, the dominance of R195, related to ethanol, decreases from pure ethanol to pure DME. On the other hand, the addition of DME makes R273, which is related to DME, more dominant.

In future work, computational studies can be conducted using different chemical kinetic mechanisms. The mechanisms mentioned in the previous sections, such as the Lawrence Livermore National Laboratory(LLNL) mechanism or the AramcoMech Mechanism from NUI Galway, can be used to reproduce the experiment results. Thus, the critical conditions of autoignition can be compared between the computational results of different mechanisms and experiment results. Consequently, it could also shed light on the subtle offset between experimental and computational results.

Bibliography

[1] A. Loukou, J. Reiter, R. Gehmlich, C. Hasse, D. Trimis, E. Pucher, and K. Seshadri, "Autoignition and extinction of mixtures of ethanol and dimethyl ether," in *Proceedings of the 7h European Combustion Meeting, Budapest, H, March 30 - April 2, 2015*, Chemol-Congress, 2015. 34.14.02; LK 01.

[2] "Chemical-kinetic mechanisms for combustion applications, San Diego mechanism web page, Mechanical and Aerospace Engineering (combustion research), University of California at San Diego." Available at http://combustion.ucsd.edu.

[3] David G. Goodwin and Harry K. Moffat and Ingmar Schoegl and Raymond L. Speth and Bryan W. Weber, "Cantera: An Object-oriented Software Toolkit for Chemical Kinetics, Thermodynamics, and Transport Processes." https://www.cantera.org, 2022. Version 2.6.0.

[4] F. Williams, *Combustion Theory; The Fundamental Theory of Chemically Reacting Flow Systems*. Reading, MA, Addison-Wesley Publishing Company, Incorporated, 1965.

[5] K. Seshadri and F. Williams, "Laminar flow between parallel plates with injection of a reactant at high reynolds number," *International Journal of Heat and Mass Transfer*, vol. 21, no. 2, pp. 251–253, 1978.

[6] R. J. Kee, J. A. Miller, G. H. Evans, and G. Dixon-Lewis, "A computational model of the structure and extinction of strained, opposed flow, premixed methane-air flames," *Symposium (International) on Combustion*, vol. 22, no. 1, pp. 1479–1494, 1989.

[7] A. E. Lutz, R. J. Kee, J. F. Grcar, and F. M. Rupley, "Oppdif: A fortran program for computing opposed-flow diffusion flames," 5 1997.

[8] G. Ribert, N. Zong, V. Yang, L. Pons, N. Darabiha, and S. Candel, "Counterflow diffusion flames of general fluids: Oxygen/hydrogen mixtures," *Combustion and Flame*, vol. 154, pp. 319–330, 08 2008.

[9] J. Li, *Experimental and numerical studies of ethanol chemical kinetics*. PhD thesis, Princeton University, NJ, United States of America, 2004.

[10] P. Saxena and F. A. Williams, "Numerical and experimental studies of ethanol flames," *Proceedings of the Combustion Institute*, vol. 31, pp. 1149–1156, Jan. 2007.

[11] J. C. Prince and F. A. Williams, “A short reaction mechanism for the combustion of dimethyl-ether,” *Combustion and Flame*, vol. 162, no. 10, pp. 3589–3595, 2015.

[12] J. C. Prince and F. A. Williams, “A short reaction mechanism for the combustion of dimethyl-ether,” *Combustion and Flame*, vol. 162, no. 10, pp. 3589–3595, 2015.

[13] U. Burke, K. P. Somers, P. O’Toole, C. M. Zinner, N. Marquet, G. Bourque, E. L. Petersen, W. K. Metcalfe, Z. Serinyel, and H. J. Curran, “An ignition delay and kinetic modeling study of methane, dimethyl ether, and their mixtures at high pressures,” *Combustion and Flame*, vol. 162, pp. 315–330, Feb. 2015.

[14] R. Seiser, H. Pitsch, K. Seshadri, W. Pitz, and H. Gurran, “Extinction and autoignition of n-heptane in counterflow configuration,” *Proceedings of the Combustion Institute*, vol. 28, no. 2, pp. 2029–2037, 2000.

[15] U. Niemann, K. Seshadri, and F. Williams, “Accuracies of laminar counterflow flame experiments,” *Combustion and Flame*, vol. 162, 12 2014.

Appendices

Appendix A

Table 1: Reactions of San Diego Mechanism

R1 :	$H+O_2 \Leftrightarrow OH+O$
R2 :	$H_2+O \Leftrightarrow OH+H$
R3 :	$H_2+OH \Leftrightarrow H_2O+H$
R4 :	$H_2O+O \Leftrightarrow_2 OH$
R5 :	$2H+M \Leftrightarrow H_2+M$
R6 :	$H+OH+M \Leftrightarrow H_2O+M$
R7 :	$2O+M \Leftrightarrow O_2+M$
R8 :	$H+O+M \Leftrightarrow OH+M$
R9 :	$H+O_2(+M) \Leftrightarrow HO_2(+M)$
R10 :	$HO_2+H \Leftrightarrow_2 OH$
R11 :	$HO_2+H \Leftrightarrow H_2+O_2$
R12 :	$HO_2+H \Leftrightarrow H_2O+O$
R13 :	$HO_2+O \Leftrightarrow OH+O_2$
R14 :	$HO_2+OH \Leftrightarrow H_2O+O_2$
R15 :	$HO_2+OH \Leftrightarrow H_2O+O_2$
R16 :	$2OH(+M) \Leftrightarrow H_2O_2(+M)$
R17 :	$2HO_2 \Leftrightarrow H_2O_2+O_2$
R18 :	$2HO_2 \Leftrightarrow H_2O_2+O_2$
R19 :	$H_2O_2+H \Leftrightarrow HO_2+H_2$
R20 :	$H_2O_2+H \Leftrightarrow H_2O+OH$
R21 :	$H_2O_2+OH \Leftrightarrow H_2O+HO_2$
R22 :	$H_2O_2+OH \Leftrightarrow H_2O+HO_2$

Continued on next page

Table 1: Reactions of San Diego Mechanism (Continued)

R23 :	$H_2O_2 + O \Leftrightarrow HO_2 + OH$
R24 :	$CO + O(+M) \Leftrightarrow CO_2(+M)$
R25 :	$CO + OH \Leftrightarrow CO_2 + H$
R26 :	$CO + HO_2 \Leftrightarrow CO_2 + OH$
R27 :	$CO + O_2 \Leftrightarrow CO_2 + O$
R28 :	$HCO + M \Leftrightarrow CO + H + M$
R29 :	$HCO + H \Leftrightarrow CO + H_2$
R30 :	$HCO + O \Leftrightarrow CO + OH$
R31 :	$HCO + O \Leftrightarrow CO_2 + H$
R32 :	$HCO + OH \Leftrightarrow CO + H_2O$
R33 :	$HCO + O_2 \Leftrightarrow CO + HO_2$
R34 :	$HCO + CH_3 \Leftrightarrow CO + CH_4$
R35 :	$H + HCO(+M) \Leftrightarrow CH_2O(+M)$
R36 :	$CH_2O + H \Leftrightarrow HCO + H_2$
R37 :	$CH_2O + O \Leftrightarrow HCO + OH$
R38 :	$CH_2O + OH \Leftrightarrow HCO + H_2O$
R39 :	$CH_2O + O_2 \Leftrightarrow HCO + HO_2$
R40 :	$CH_2O + HO_2 \Leftrightarrow HCO + H_2O_2$
R41 :	$CH_4 + H \Leftrightarrow H_2 + CH_3$
R42 :	$CH_4 + OH \Leftrightarrow H_2O + CH_3$
R43 :	$CH_4 + O \Leftrightarrow CH_3 + OH$
R44 :	$CH_4 + O_2 \Leftrightarrow CH_3 + HO_2$
R45 :	$CH_4 + HO_2 \Leftrightarrow CH_3 + H_2O_2$
R46 :	$CH_3 + H \Leftrightarrow T - CH_2 + H_2$
R47 :	$CH_3 + H \Leftrightarrow S - CH_2 + H_2$
R48 :	$CH_3 + OH \Leftrightarrow S - CH_2 + H_2O$
R49 :	$CH_3 + O \Leftrightarrow CH_2O + H$
R50 :	$CH_3 + T - CH_2 \Leftrightarrow C_2H_4 + H$
R51 :	$CH_3 + HO_2 \Leftrightarrow CH_3O + OH$
R52 :	$CH_3 + O_2 \Leftrightarrow CH_2O + OH$

Continued on next page

Table 1: Reactions of San Diego Mechanism (Continued)

R53 :	$CH_3+O_2 \Leftrightarrow CH_3O+O$
R54 :	$2CH_3 \Leftrightarrow C_2H_4+H_2$
R55 :	$2CH_3 \Leftrightarrow C_2H_5+H$
R56 :	$H+CH_3(+M) \Leftrightarrow CH_4(+M)$
R57 :	$2CH_3(+M) \Leftrightarrow C_2H_6(+M)$
R58 :	$S-CH_2+OH \Leftrightarrow CH_2O+H$
R59 :	$S-CH_2+O_2 \Leftrightarrow CO+OH+H$
R60 :	$S-CH_2+CO_2 \Leftrightarrow CO+CH_2O$
R61 :	$S-CH_2+M \Leftrightarrow T-CH_2+M$
R62 :	$T-CH_2+H \Leftrightarrow CH+H_2$
R63 :	$T-CH_2+OH \Leftrightarrow CH_2O+H$
R64 :	$T-CH_2+OH \Leftrightarrow CH+H_2O$
R65 :	$T-CH_2+O \Leftrightarrow CO+_2H$
R66 :	$T-CH_2+O \Leftrightarrow CO+H_2$
R67 :	$T-CH_2+O_2 \Leftrightarrow CO_2+H_2$
R68 :	$T-CH_2+O_2 \Leftrightarrow CO+OH+H$
R69 :	$2T-CH_2 \Leftrightarrow C_2H_2+_2H$
R70 :	$C_2H_2+HO_2 \Leftrightarrow CHCHO+OH$
R71 :	$CHCHO+O_2 \Leftrightarrow CH_2O+CO+O$
R72 :	$CH+O \Leftrightarrow CO+H$
R73 :	$CH+O_2 \Leftrightarrow HCO+O$
R74 :	$CH+H_2O \Leftrightarrow CH_2O+H$
R75 :	$CH+CO_2 \Leftrightarrow HCO+CO$
R76 :	$CH_3O+H \Leftrightarrow CH_2O+H_2$
R77 :	$CH_3O+H \Leftrightarrow S-CH_2+H_2O$
R78 :	$CH_3O+OH \Leftrightarrow CH_2O+H_2O$
R79 :	$CH_3O+O \Leftrightarrow OH+CH_2O$
R80 :	$CH_3O+O_2 \Leftrightarrow CH_2O+HO_2$
R81 :	$CH_3O+M \Leftrightarrow CH_2O+H+M$
R82 :	$C_2H_6+H \Leftrightarrow C_2H_5+H_2$

Continued on next page

Table 1: Reactions of San Diego Mechanism (Continued)

R83 :	$C_2H_6+O \Leftrightarrow C_2H_5+OH$
R84 :	$C_2H_6+OH \Leftrightarrow C_2H_5+H_2O$
R85 :	$C_2H_6+CH_3 \Leftrightarrow C_2H_5+CH_4$
R86 :	$C_2H_6(+M) \Leftrightarrow C_2H_5+H(+M)$
R87 :	$C_2H_6+HO_2 \Leftrightarrow C_2H_5+H_2O_2$
R88 :	$C_2H_5+H \Leftrightarrow C_2H_4+H_2$
R89 :	$C_2H_5+O \Leftrightarrow C_2H_4+OH$
R90 :	$C_2H_5+O \Leftrightarrow CH_3+CH_2O$
R91 :	$C_2H_5+O_2 \Leftrightarrow C_2H_4+HO_2$
R92 :	$C_2H_5+O_2 \Leftrightarrow C_2H_4OOH$
R93 :	$C_2H_4OOH \Leftrightarrow C_2H_4+HO_2$
R94 :	$C_2H_4OOH+O_2 \Leftrightarrow OC_2H_3OOH+OH$
R95 :	$OC_2H_3OOH \Leftrightarrow CH_2O+HCO+OH$
R96 :	$C_2H_5(+M) \Leftrightarrow C_2H_4+H(+M)$
R97 :	$C_2H_4+H \Leftrightarrow C_2H_3+H_2$
R98 :	$C_2H_4+OH \Leftrightarrow C_2H_3+H_2O$
R99 :	$C_2H_4+O \Leftrightarrow CH_3+HCO$
R100 :	$C_2H_4+O \Leftrightarrow CH_2CHO+H$
R101 :	$_2C_2H_4 \Leftrightarrow C_2H_3+C_2H_5$
R102 :	$C_2H_4+O_2 \Leftrightarrow C_2H_3+HO_2$
R103 :	$C_2H_4+HO_2 \Leftrightarrow C_2H_4O+OH$
R104 :	$C_2H_4O+HO_2 \Leftrightarrow CH_3+CO+H_2O_2$
R105 :	$C_2H_4+M \Leftrightarrow C_2H_3+H+M$
R106 :	$C_2H_4+M \Leftrightarrow C_2H_2+H_2+M$
R107 :	$C_2H_3+H \Leftrightarrow C_2H_2+H_2$
R108 :	$C_2H_3(+M) \Leftrightarrow C_2H_2+H(+M)$
R109 :	$C_2H_3+O_2 \Leftrightarrow CH_2O+HCO$
R110 :	$C_2H_3+O_2 \Leftrightarrow CH_2CHO+O$
R111 :	$C_2H_3+O_2 \Leftrightarrow C_2H_2+HO_2$
R112 :	$C_2H_2+O \Leftrightarrow HCCO+H$

Continued on next page

Table 1: Reactions of San Diego Mechanism (Continued)

R113 :	$C_2H_2 + O \Leftrightarrow T - CH_2 + CO$
R114 :	$C_2H_2 + O_2 \Leftrightarrow CH_2O + CO$
R115 :	$C_2H_2 + OH \Leftrightarrow CH_2CO + H$
R116 :	$C_2H_2 + OH \Leftrightarrow C_2H + H_2O$
R117 :	$CH_2CO + H \Leftrightarrow CH_3 + CO$
R118 :	$CH_2CO + O \Leftrightarrow T - CH_2 + CO_2$
R119 :	$CH_2CO + O \Leftrightarrow HCCO + OH$
R120 :	$CH_2CO + CH_3 \Leftrightarrow C_2H_5 + CO$
R121 :	$HCCO + H \Leftrightarrow S - CH_2 + CO$
R122 :	$HCCO + OH \Leftrightarrow HCO + CO + H$
R123 :	$HCCO + O \Leftrightarrow_2 CO + H$
R124 :	$HCCO + O_2 \Leftrightarrow_2 CO + OH$
R125 :	$HCCO + O_2 \Leftrightarrow CO_2 + CO + H$
R126 :	$C_2H + OH \Leftrightarrow HCCO + H$
R127 :	$C_2H + O \Leftrightarrow CO + CH$
R128 :	$C_2H + O_2 \Leftrightarrow HCCO + O$
R129 :	$C_2H + O_2 \Leftrightarrow CH + CO_2$
R130 :	$C_2H + O_2 \Leftrightarrow HCO + CO$
R131 :	$CH_2OH + H \Leftrightarrow CH_2O + H_2$
R132 :	$CH_2OH + H \Leftrightarrow CH_3 + OH$
R133 :	$CH_2OH + OH \Leftrightarrow CH_2O + H_2O$
R134 :	$CH_2OH + O_2 \Leftrightarrow CH_2O + HO_2$
R135 :	$CH_2OH + M \Leftrightarrow CH_2O + H + M$
R136 :	$CH_3O + M \Leftrightarrow CH_2OH + M$
R137 :	$CH_2CO + OH \Leftrightarrow CH_2OH + CO$
R138 :	$CH_3OH + OH \Leftrightarrow CH_2OH + H_2O$
R139 :	$CH_3OH + OH \Leftrightarrow CH_3O + H_2O$
R140 :	$CH_3OH + H \Leftrightarrow CH_2OH + H_2$
R141 :	$CH_3OH + H \Leftrightarrow CH_3O + H_2$
R142 :	$CH_3OH + O \Leftrightarrow CH_2OH + OH$

Continued on next page

Table 1: Reactions of San Diego Mechanism (Continued)

R143 :	$CH_3OH + HO_2 \Leftrightarrow CH_2OH + H_2O_2$
R144 :	$CH_3OH + O_2 \Leftrightarrow CH_2OH + HO_2$
R145 :	$CH_3OH(+M) \Leftrightarrow CH_3 + OH(+M)$
R146 :	$CH_2CHO \Leftrightarrow CH_2CO + H$
R147 :	$CH_2CHO + H \Leftrightarrow CH_3 + HCO$
R148 :	$CH_2CHO + H \Leftrightarrow CH_2CO + H_2$
R149 :	$CH_2CHO + O \Leftrightarrow CH_2O + HCO$
R150 :	$CH_2CHO + OH \Leftrightarrow CH_2CO + H_2O$
R151 :	$CH_2CHO + O_2 \Leftrightarrow CH_2O + CO + OH$
R152 :	$CH_2CHO + CH_3 \Leftrightarrow C_2H_5 + CO + H$
R153 :	$CH_2CHO + HO_2 \Leftrightarrow CH_2O + HCO + OH$
R154 :	$CH_2CHO + HO_2 \Leftrightarrow CH_3CHO + O_2$
R155 :	$CH_2CHO \Leftrightarrow CH_3 + CO$
R156 :	$CH_3CHO \Leftrightarrow CH_3 + HCO$
R157 :	$CH_3CO(+M) \Leftrightarrow CH_3 + CO(+M)$
R158 :	$CH_3CHO + OH \Leftrightarrow CH_3CO + H_2O$
R159 :	$CH_3CHO + OH \Leftrightarrow CH_2CHO + H_2O$
R160 :	$CH_3CHO + O \Leftrightarrow CH_3CO + OH$
R161 :	$CH_3CHO + O \Leftrightarrow CH_2CHO + OH$
R162 :	$CH_3CHO + H \Leftrightarrow CH_3CO + H_2$
R163 :	$CH_3CHO + H \Leftrightarrow CH_2CHO + H_2$
R164 :	$CH_3CHO + CH_3 \Leftrightarrow CH_3CO + CH_4$
R165 :	$CH_3CHO + CH_3 \Leftrightarrow CH_2CHO + CH_4$
R166 :	$CH_3CHO + HO_2 \Leftrightarrow CH_3CO + H_2O_2$
R167 :	$CH_3CHO + HO_2 \Leftrightarrow CH_2CHO + H_2O_2$
R168 :	$CH_3CHO + O_2 \Leftrightarrow CH_3CO + HO_2$
R169 :	$C_2H_5OH(+M) \Leftrightarrow CH_3 + CH_2OH(+M)$
R170 :	$C_2H_5OH(+M) \Leftrightarrow C_2H_4 + H_2O(+M)$
R171 :	$C_2H_5OH + OH \Leftrightarrow CH_2CH_2OH + H_2O$
R172 :	$C_2H_5OH + OH \Leftrightarrow CH_3CHOH + H_2O$

Continued on next page

Table 1: Reactions of San Diego Mechanism (Continued)

R173 :	$C_2H_5OH+OH \Leftrightarrow CH_3CH_2O+H_2O$
R174 :	$C_2H_5OH+H \Leftrightarrow CH_2CH_2OH+H_2$
R175 :	$C_2H_5OH+H \Leftrightarrow CH_3CHOH+H_2$
R176 :	$C_2H_5OH+H \Leftrightarrow CH_3CH_2O+H_2$
R177 :	$C_2H_5OH+O \Leftrightarrow CH_2CH_2OH+OH$
R178 :	$C_2H_5OH+O \Leftrightarrow CH_3CHOH+OH$
R179 :	$C_2H_5OH+O \Leftrightarrow CH_3CH_2O+OH$
R180 :	$C_2H_5OH+CH_3 \Leftrightarrow CH_2CH_2OH+CH_4$
R181 :	$C_2H_5OH+CH_3 \Leftrightarrow CH_3CHOH+CH_4$
R182 :	$C_2H_5OH+CH_3 \Leftrightarrow CH_3CH_2O+CH_4$
R183 :	$C_2H_5OH+HO_2 \Leftrightarrow CH_3CHOH+H_2O_2$
R184 :	$C_2H_5OH+HO_2 \Leftrightarrow CH_2CH_2OH+H_2O_2$
R185 :	$C_2H_5OH+HO_2 \Leftrightarrow CH_3CH_2O+H_2O_2$
R186 :	$C_2H_4+OH \Leftrightarrow CH_2CH_2OH$
R187 :	$C_2H_5+HO_2 \Leftrightarrow CH_3CH_2O+OH$
R188 :	$CH_3CH_2O+M \Leftrightarrow CH_3CHO+H+M$
R189 :	$CH_3CH_2O+M \Leftrightarrow CH_3+CH_2O+M$
R190 :	$CH_3CH_2O+O_2 \Leftrightarrow CH_3CHO+HO_2$
R191 :	$CH_3CH_2O+CO \Leftrightarrow C_2H_5+CO_2$
R192 :	$CH_3CH_2O+H \Leftrightarrow CH_3+CH_2OH$
R193 :	$CH_3CH_2O+H \Leftrightarrow C_2H_4+H_2O$
R194 :	$CH_3CH_2O+OH \Leftrightarrow CH_3CHO+H_2O$
R195 :	$CH_3CHOH+O_2 \Leftrightarrow CH_3CHO+HO_2$
R196 :	$CH_3CHOH+O \Leftrightarrow CH_3CHO+OH$
R197 :	$CH_3CHOH+H \Leftrightarrow C_2H_4+H_2O$
R198 :	$CH_3CHOH+H \Leftrightarrow CH_3+CH_2OH$
R199 :	$CH_3CHOH+HO_2 \Leftrightarrow CH_3CHO+_2OH$
R200 :	$CH_3CHOH+OH \Leftrightarrow CH_3CHO+H_2O$
R201 :	$CH_3CHOH+M \Leftrightarrow CH_3CHO+H+M$
R202 :	$C_3H_4+O \Leftrightarrow C_2H_4+CO$

Continued on next page

Table 1: Reactions of San Diego Mechanism (Continued)

R203 :	$CH_3 + C_2H_2 \Leftrightarrow C_3H_4 + H$
R204 :	$C_3H_4 + O \Leftrightarrow HCCO + CH_3$
R205 :	$C_3H_3 + H(+M) \Leftrightarrow C_3H_4(+M)$
R206 :	$C_3H_3 + HO_2 \Leftrightarrow C_3H_4 + O_2$
R207 :	$C_3H_4 + OH \Leftrightarrow C_3H_3 + H_2O$
R208 :	$C_3H_3 + O_2 \Leftrightarrow CH_2CO + HCO$
R209 :	$C_3H_4 + H(+M) \Leftrightarrow C_3H_5(+M)$
R210 :	$C_3H_5 + H \Leftrightarrow C_3H_4 + H_2$
R211 :	$C_3H_5 + O_2 \Leftrightarrow C_3H_4 + HO_2$
R212 :	$C_3H_5 + CH_3 \Leftrightarrow C_3H_4 + CH_4$
R213 :	$C_2H_2 + CH_3(+M) \Leftrightarrow C_3H_5(+M)$
R214 :	$C_3H_5 + OH \Leftrightarrow C_3H_4 + H_2O$
R215 :	$C_3H_3 + HCO \Leftrightarrow C_3H_4 + CO$
R216 :	$C_3H_3 + HO_2 \Leftrightarrow OH + CO + C_2H_3$
R217 :	$C_3H_4 + O_2 \Leftrightarrow CH_3 + HCO + CO$
R218 :	$C_3H_6 + O \Leftrightarrow C_2H_5 + HCO$
R219 :	$C_3H_6 + OH \Leftrightarrow C_3H_5 + H_2O$
R220 :	$C_3H_6 + O \Leftrightarrow CH_2CO + CH_3 + H$
R221 :	$C_3H_6 + H \Leftrightarrow C_3H_5 + H_2$
R222 :	$C_3H_5 + H(+M) \Leftrightarrow C_3H_6(+M)$
R223 :	$C_3H_5 + HO_2 \Leftrightarrow C_3H_6 + O_2$
R224 :	$C_3H_5 + HO_2 \Leftrightarrow OH + C_2H_3 + CH_2O$
R225 :	$C_2H_3 + CH_3(+M) \Leftrightarrow C_3H_6(+M)$
R226 :	$C_3H_6 + H \Leftrightarrow C_2H_4 + CH_3$
R227 :	$CH_3 + C_2H_3 \Leftrightarrow C_3H_5 + H$
R228 :	$C_3H_8(+M) \Leftrightarrow CH_3 + C_2H_5(+M)$
R229 :	$C_3H_8 + O_2 \Leftrightarrow I - C_3H_7 + HO_2$
R230 :	$C_3H_8 + O_2 \Leftrightarrow N - C_3H_7 + HO_2$
R231 :	$C_3H_8 + H \Leftrightarrow I - C_3H_7 + H_2$
R232 :	$C_3H_8 + H \Leftrightarrow N - C_3H_7 + H_2$

Continued on next page

Table 1: Reactions of San Diego Mechanism (Continued)

R233 :	$C_3H_8 + O \Leftrightarrow I - C_3H_7 + OH$
R234 :	$C_3H_8 + O \Leftrightarrow N - C_3H_7 + OH$
R235 :	$C_3H_8 + OH \Leftrightarrow N - C_3H_7 + H_2O$
R236 :	$C_3H_8 + OH \Leftrightarrow I - C_3H_7 + H_2O$
R237 :	$C_3H_8 + HO_2 \Leftrightarrow I - C_3H_7 + H_2O_2$
R238 :	$C_3H_8 + HO_2 \Leftrightarrow N - C_3H_7 + H_2O_2$
R239 :	$I - C_3H_7 + C_3H_8 \Leftrightarrow N - C_3H_7 + C_3H_8$
R240 :	$C_3H_6 + H(+M) \Leftrightarrow I - C_3H_7(+M)$
R241 :	$I - C_3H_7 + O_2 \Leftrightarrow C_3H_6 + HO_2$
R242 :	$N - C_3H_7(+M) \Leftrightarrow CH_3 + C_2H_4(+M)$
R243 :	$H + C_3H_6(+M) \Leftrightarrow N - C_3H_7(+M)$
R244 :	$N - C_3H_7 + O_2 \Leftrightarrow C_3H_6 + HO_2$
R245 :	$N - C_3H_7 + O_2 \Leftrightarrow C_3H_6OOH$
R246 :	$C_3H_6OOH \Leftrightarrow C_3H_6 + HO_2$
R247 :	$C_3H_6OOH + O_2 \Leftrightarrow OC_3H_5OOH + OH$
R248 :	$OC_3H_5OOH \Leftrightarrow CH_2CHO + CH_2O + OH$
R249 :	$C_4H_{10}(+M) \Leftrightarrow_2 C_2H_5(+M)$
R250 :	$C_4H_{10} + O_2 \Leftrightarrow PC_4H_9 + HO_2$
R251 :	$C_4H_{10} + O_2 \Leftrightarrow SC_4H_9 + HO_2$
R252 :	$C_4H_{10} + HO_2 \Leftrightarrow PC_4H_9 + H_2O_2$
R253 :	$C_4H_{10} + HO_2 \Leftrightarrow SC_4H_9 + H_2O_2$
R254 :	$C_4H_{10} + O \Leftrightarrow PC_4H_9 + OH$
R255 :	$C_4H_{10} + O \Leftrightarrow SC_4H_9 + OH$
R256 :	$C_4H_{10} + OH \Leftrightarrow PC_4H_9 + H_2O$
R257 :	$C_4H_{10} + OH \Leftrightarrow SC_4H_9 + H_2O$
R258 :	$C_4H_{10} + H \Leftrightarrow H_2 + PC_4H_9$
R259 :	$C_4H_{10} + H \Leftrightarrow H_2 + SC_4H_9$
R260 :	$PC_4H_9 \Leftrightarrow C_2H_5 + C_2H_4$
R261 :	$SC_4H_9 \Leftrightarrow C_3H_6 + CH_3$
R262 :	$C_4H_8 \Leftrightarrow C_3H_5 + CH_3$

Continued on next page

Table 1: Reactions of San Diego Mechanism (Continued)

R263 :	$C_4H_8 + H \Leftrightarrow H_2 + C_2H_3 + C_2H_4$
R264 :	$SC_4H_9 + O_2 \Leftrightarrow SC_4H_9O_2$
R265 :	$SC_4H_9O_2 \Leftrightarrow C_4H_8 + HO_2$
R266 :	$PC_4H_9 + O_2 \Leftrightarrow C_4H_8 + HO_2$
R267 :	$PC_4H_9 + O_2 \Leftrightarrow C_4H_8OOH1-_3$
R268 :	$C_4H_8OOH1-_3 \Leftrightarrow C_4H_8 + HO_2$
R269 :	$C_4H_8OOH1-_3 + O_2 \Leftrightarrow NC_4KET1_3 + OH$
R270 :	$NC_4KET1_3 \Leftrightarrow N - C_3H_7 + CO_2 + OH$
R271 :	$CH_3OCH_3(+M) \Leftrightarrow CH_3O + CH_3(+M)$
R272 :	$CH_3OCH_3 + O_2 \Leftrightarrow CH_3OCH_2 + HO_2$
R273 :	$CH_3OCH_3 + OH \Leftrightarrow CH_3OCH_2 + H_2O$
R274 :	$CH_3OCH_3 + CH_3 \Leftrightarrow CH_3OCH_2 + CH_4$
R275 :	$CH_3OCH_3 + H \Leftrightarrow CH_3OCH_2 + H_2$
R276 :	$CH_3OCH_3 + HO_2 \Leftrightarrow CH_3OCH_2 + H_2O_2$
R277 :	$CH_3OCH_2 \Leftrightarrow CH_2O + CH_3$
R278 :	$CH_3OCH_2 + O_2 \Leftrightarrow CH_2O + CH_2O + OH$
R279 :	$CH_3OCH_2 + O_2 \Leftrightarrow CH_3OCH_2O_2$
R280 :	$CH_3OCH_2O_2 + CH_3OCH_2O_2 \Leftrightarrow O_2 + 2CH_3O + 2CH_2O$
R281 :	$CH_3OCH_2O_2 \Leftrightarrow CH_2OCH_2O_2H$
R282 :	$CH_2OCH_2O_2H \Leftrightarrow CH_2O + CH_2O + OH$
R283 :	$CH_2OCH_2O_2H + O_2 \Leftrightarrow HO_2CH_2OCHO + OH$
R284 :	$HO_2CH_2OCHO \Leftrightarrow CH_2O + CO_2 + OH + H$